Receptor-driven, multimodal mapping of the human amygdala

Olga Kedo, Karl Zilles, Nicola Palomero-Gallagher, Axel Schleicher, Hartmut Mohlberg, Sebastian Bludau & Katrin Amunts

Brain Structure and Function

ISSN 1863-2653
Volume 223
Number 4

Brain Struct Funct (2018) 223:1637-1666
DOI 10.1007/s00429-017-1577-x

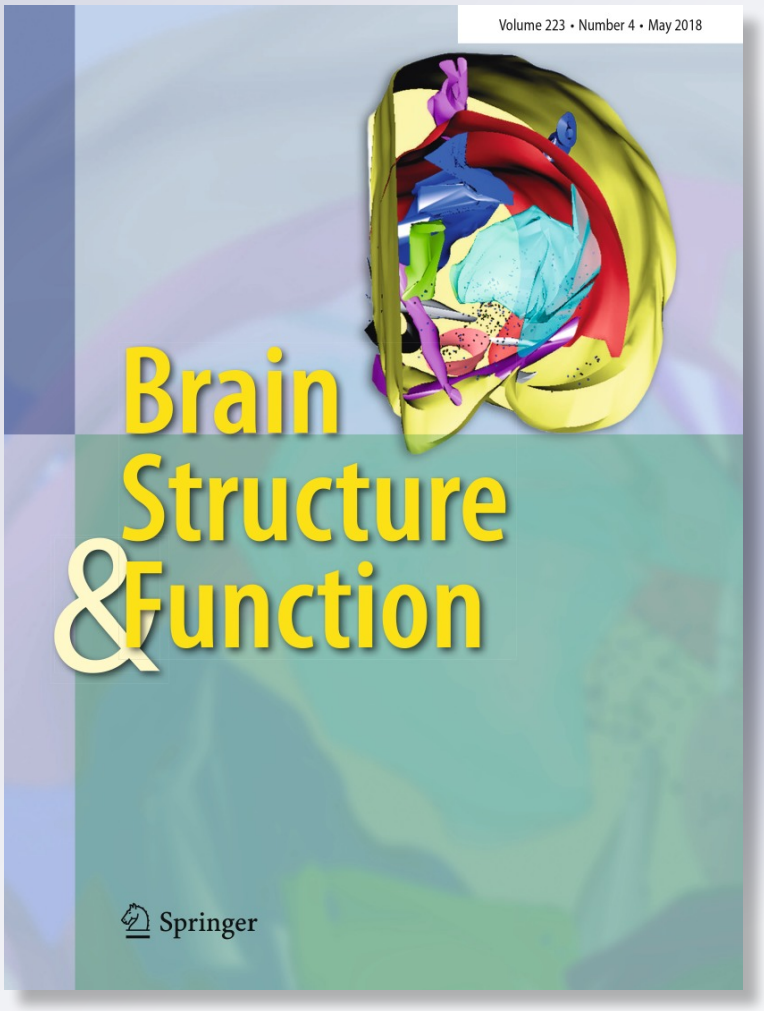

Springer

Brain Structure and Function (2018) 223:1637–1666
https://doi.org/10.1007/s00429-017-1577-x

ORIGINAL ARTICLE

Receptor-driven, multimodal mapping of the human amygdala

Olga Kedo[1] · Karl Zilles[1,2,3] · Nicola Palomero-Gallagher[1] · Axel Schleicher[1] · Hartmut Mohlberg[1] · Sebastian Bludau[1] · Katrin Amunts[1,3,4]

Received: 13 February 2017 / Accepted: 20 November 2017 / Published online: 29 November 2017

Abstract
The human amygdala consists of subdivisions contributing to various functions. However, principles of structural organization at the cellular and molecular level are not well understood. Thus, we re-analyzed the cytoarchitecture of the amygdala and generated cytoarchitectonic probabilistic maps of ten subdivisions in stereotaxic space based on novel workflows and mapping tools. This parcellation was then used as a basis for analyzing the receptor expression for 15 receptor types. Receptor fingerprints, i.e., the characteristic balance between densities of all receptor types, were generated in each subdivision to comprehensively visualize differences and similarities in receptor architecture between the subdivisions. Fingerprints of the central and medial nuclei and the anterior amygdaloid area were highly similar. Fingerprints of the lateral, basolateral and basomedial nuclei were also similar to each other, while those of the remaining nuclei were distinct in shape. Similarities were further investigated by a hierarchical cluster analysis: a two-cluster solution subdivided the phylogenetically older part (central, medial nuclei, anterior amygdaloid area) from the remaining parts of the amygdala. A more fine-grained three-cluster solution replicated our previous parcellation including a laterobasal, superficial and centromedial group. Furthermore, it helped to better characterize the paralaminar nucleus with a molecular organization in-between the laterobasal and the superficial group. The multimodal cyto- and receptor-architectonic analysis of the human amygdala provides new insights into its microstructural organization, intersubject variability, localization in stereotaxic space and principles of receptor-based neurochemical differences.

Keywords Amygdala · Cytoarchitecture · Probabilistic mapping · Receptor architecture · Human brain

Introduction

The human amygdala is involved in processing of emotions, social cognition, olfaction, learning, vegetative and other functions (LeDoux 2000; Adolphs 2010; Olsson and Phelps 2007; Talarovicova et al. 2007; Soudry et al. 2011; Canessa et al. 2013; Hesse et al. 2016). Since neurotransmitter receptors are key molecules of signal transmission, their expression in the amygdala is important for its functional diversity. It has been demonstrated that glutamatergic AMPA and NMDA as well as dopaminergic D_1 receptors are involved in different aspects of fear processing (Walker and Davis 2002; Guarraci et al. 1999; Takahashi et al. 2012). Serotonin 5-HT_{1A} receptor knockout mice show a decreased exploratory activity and increased fear reaction to aversive events (Ramboz et al. 1998). Furthermore, a low-fear phenotype in a patient with Urbach–Wiethe disease with selective bilateral amygdala damage is associated with a 70% global decrease in the binding potential of 5-HT_{2A} receptors throughout the brain (Hurlemann et al. 2009). Stimulation of 5-HT_{2A} receptors on GABAergic interneurons of the amygdala and hippocampus lead to increased GABA release, and thereby modulate synchronized rhythmic activity during memory formation (Bombardi and Di Giovanni 2013). Stressful events, such as conditioned fear, cause significant

✉ Olga Kedo
o.kedo@fz-juelich.de

1 Institute of Neuroscience and Medicine, INM-1, Research Centre Jülich, Jülich, Germany

2 Department of Psychiatry, Psychotherapy and Psychosomatics, RWTH Aachen University, Aachen, Germany

3 JARA-BRAIN, Jülich-Aachen Research Alliance, Aachen, Germany

4 C. & O. Vogt Institute for Brain Research, University Hospital Düsseldorf, Heinrich Heine University Düsseldorf, Düsseldorf, Germany

increases in noradrenaline release in the amygdala, hypothalamus and locus coeruleus; this increase in noradrenaline release is significantly attenuated by pretreatment with diazepam in a flumazenil reversible manner, acting via the benzodiazepine/$GABA_A$ receptor complex (Tanaka et al. 2000).

Neurotransmitter receptors are differentially distributed across the human amygdala, as demonstrated for selected receptor types (e.g., Cortés et al. 1987; Niehoff and Whitehouse 1983; Pazos et al. 1987a, b). These and cytoarchitectonic as well as immunohistochemical studies on the heterogeneous cellular composition of the amygdala (Benzing et al. 1992; Brockhaus 1938; de Olmos 1990, 2004; Heimer et al. 1999; Sims and Williams 1990; Sorvari et al. 1995; Svendsen and Bird 1985; Yilmazer-Hanke 2012) resulted in parcellations into numerous subdivisions. However, details of the maps differed between the studies, e.g., as to each individual subdivision. Discrepancies regarding its existence, extent and possible sub-parcellation (see Heimer et al. 1999, Tables I–IV) as well as its nomenclature (as compared to the earlier studies, e.g., of Brockhaus 1938; Stephan 1975) hold especially true for the anterior amygdaloid area. It was not easily recognized, e.g., Yilmazer-Hanke (2012) and some earlier investigators (see Heimer et al. 1999 for comparison) identified other structures in place of AAA. The identified anterior amygdaloid area was different in its extent between the studies: AAA of de Olmos (1990, 2004) constituted only a part of AA of Sims and Williams (1990). Moreover, de Olmos further subdivided this area into the superficial (AAAsf) and deep (AAAdp) parts in contrast to the latter authors. Sometimes the nomenclature and classification of the amygdaloid subdivisions seems to be confusing because nearly similar terms were used for different structures, e.g., 'the parahippocampal–amygdaloid transition area (PHA)' of Yilmazer-Hanke (2012) and the hippocampal–amygdaloid transition area (HATA) of Rosene and van Hoesen (1987), but the former is the part of the amygdala and the latter is a part of the hippocampus. Most of the amygdala studies, however, do not mention the HATA. The amygdalohippocampal transition area, which is a caudal area of the amygdala at the border with HATA, is also a subject of controversies: the term 'amygdalohippocampal transition area (AHi)' referred to the entire amygdaloid subdivision which included a posterodorsal(medial) and anteroventral(lateral) division in the study of de Olmos (2004). In contrast, 'amygdalohippocampal area' [AHA of Sorvari et al. (1995, 1996a, b)] refers only to the latter division of AHi as proposed by de Olmos (Heimer et al. 1999). The other example is the posterior cortical nucleus which in the study of de Olmos (1990) is comparable to a dorsal portion of the posterodorsal(medial) division of AHi (de Olmos 2004), whereas posterior cortical nucleus (COp) of Sorvari et al. corresponds to the entire posterodorsal(medial) division of AHi (Heimer et al. 1999). Other parcellation of the transitional area of the amygdala to the hippocampus includes from one [Pam Ch of Stephan (1975)] up to 4 (Brockhaus 1938) subdivisions.

Other differences in the classification schemes can also be found. The 'Supraamygdaleum' of Brockhaus (1938) segregated the anterior amygdaloid area along with central and medial nuclei from the amygdala proper ('Amygdaleum proprium'). The anterior amygdaloid area was included to the olfactory amygdala along with the subdivisions of the superficial amygdala (de Olmos 1990), while later it was considered as a part of the extended amygdala along with the centromedial amygdala (de Olmos 2004). The paralaminar nucleus was considered to be part of the basolateral nucleus (de Olmos 1990; Sims and Williams 1990), or interpreted as an individual subdivision (de Olmos 2004; Heimer et al. 1999).

In order to address such controversies and even confusion, it would be necessary to rely a classification of subdivisions on quantitative and reproducible measures of similarities between the subdivisions. To introduce such metrics has not been possible in the past considering the largely qualitative analysis of cellular architecture without considering other modalities.

Our previous cytoarchitectonic work has identified subdivisions of the amygdala with a focus on their grouping: (1) *the superficial group* contained the anterior amygdaloid area, the amygdalopiriform transition area, the amygdalohippocampal transition area, the posterior cortical nucleus and the ventral cortical nuclei with its parcellations; (2) *the laterobasal group* encompassed the lateral, basolateral, basomedial and paralaminar nuclei; and (3) the *centromedial group* included the central and medial nuclei (Amunts et al. 2005; Heimer et al. 1999).

The subdivisions are involved in different functions, which partly seem to overlap [e.g., in form of functional redundancy of the basolateral and basomedial nuclei in the conditioned fear expression and extinction (Amano et al. 2011)]. Considering the fact that functions may go beyond a single subdivision, probabilistic maps were generated for the three major amygdaloid groups in order to provide a mean for assignment of findings from neuroimaging studies of the living human brain to these microanatomically defined groups, and thus, to better understand the relationship between the cytoarchitecture of the amygdala and the broad range of functions (Amunts et al. 2005). As a result, subsequent studies showed that some of the functions were spread over more than one amygdaloid group (e.g., Ball et al. 2007; Hurlemann et al. 2008; Fruhholz and Grandjean 2013), whereas the others were confined to specific groups of the amygdala (Fruhholz and Grandjean 2013; Goossens et al. 2009; Klumpers et al. 2015; Koelsch et al. 2013; Simons et al. 2014), e.g., in the study of Fruhholz and Grandjean (2013), sensitivity of functional activity

to emotional cues from speech prosody relied on both the superficial (bilaterally) and laterobasal (right) amygdaloid groups, but explicit attention to prosody implicated the laterobasal group. Also, functional characterization of the three connectivity-derived clusters of the histologically defined amygdala, which were highly concordant to the parcellation of Amunts et al. (2005), revealed both common and specific functions of each cluster (Bzdok et al. 2013). Processing of emotions, and especially fear, is a function which was linked to all three major clusters. Specific function, e.g., of the centromedial group cluster was related by the latter authors to mediating attentional, vegetative and motor responses.

The subdivisions of the amygdala reveal distinct connectivity (Price et al. 1987; Amaral et al. 1992; Fudge and Tucker 2009; Stefanacci and Amaral 2002) and specific functions in the animal studies (e.g., Amano et al. 2011; Holland and Gallagher 1999; Kalin et al. 2004). Therefore, these results suggest specific functions of the subdivisions in the human amygdala. Fruhholz and Grandjean (2013) report functional activation within a certain amygdaloid group in form of segregated clusters which may imply a more fine-grained parcellation of the amygdala, e.g., dorsal and medial clusters in the left superficial group, and dorsal and ventral clusters in the right superficial group, as well as lateral cluster in the right laterobasal group were functionally involved as a reaction on angry voices. However, a possibility to study functions at the fine-grained level is still missing in the humans.

The present study, therefore, (1) provides a refined cytoarchitectonic analysis of the parcellation of the amygdala and (2) generates the probability maps for further structure-functional correlations reflecting the intersubject variability of subdivisions of the amygdala using an improved workflow and mapping tools. This parcellation is used as basis for a regionally specific analysis of the expression of multiple receptors in the human amygdala. The balance between the densities of the different receptor types is visualized as 'multi-receptor fingerprint' in each subdivision, and the different fingerprints are further analyzed by means of a hierarchical cluster analysis, to reveal grouping of subdivisions based on the molecular organization of the amygdala.

Materials and methods

Subjects (postmortem brains)

Two samples of postmortem brains (Table 1) were used in the study. The sample 1 included ten postmortem brains (five females, five males; age range 37–86 years) which were the same as in the prior cytoarchitectonic study (Amunts et al. 2005), except for the brain number pm2, which was included in the present (but not the previous) study; the reason was that, in addition to cell body-stained sections, neighboring sections stained for myelin (Gallyas 1979) were available in this additional brain. Myelin-stained sections of pm2 (and

Table 1 Samples of the postmortem brains for the cyto- and receptor-architectonic mapping

Case	Brain/hemisphere	Cause of death	Gender	Fresh brain weight (g)	Age at death (years)	Postmortem latency (h)	Analysis
Sample 1							
1	pm 1/R, L	Carcinoma of the bladder	f	1350	79	24	C, M
2	pm 2/R, L	Carcinoma of the rectum	m	1270	56	24	C, M
3	pm 3/R, L	Cardiovascular disease	m	1360	69	16	C
4	pm 4/R, L	Toxic glomerulonephritis	m	1349	75	24	C
5	pm 5/R, L	Cardiorespiratory insufficiency	f	1142	59	24	C
6	pm 7/R, L	Right heart failure	m	1437	37	24	C
7	pm 8/R, L	Renal failure	f	1216	72	12	C
8	pm 9/R, L	Cardiorespiratory insufficiency	f	1110	79	16	C
9	pm 13/ R, L	Drowning	m	1234	39	10	C
10	pm 14/ R, L	Cardiorespiratory insufficiency	f	1113	86	24	C
Sample 2							
1	rpm1/R	Malignant melanoma	f	1326	72	8	C, M, R
2	rpm2/R, L	Pulmonary edema	m	1128	77	18	C, M, R
3	MR1/R	Multiorgan dysfunction	m	1326	78	12	C, M, R
4	MR2/L	Respiratory insufficience	f	1280	75	16	C, M, R
5	MR3/R	Sudden cardiac death	m	1477	79	12	C, M, R

R receptor-architectonic analysis, *C* cytoarchitectonic analysis, *M* myeloarchitectonic analysis (additional verification of the borders), *R* right hemisphere, *L* left hemisphere, *f* female, *m* male

pm1) were used for verification of fiber bundles. The sample 2 consisted of six deep-frozen hemispheres from five postmortem human brains (two females, three males; age range 72–79 years).

All brains were obtained from the body donor program of the Anatomical Institute of the University of Düsseldorf according to legal requirements and in accordance with the Ethical committee of Düsseldorf University and came from subjects with no history of neurological or psychiatric disorders.

Cytoarchitectonic mapping

Histological processing

Cytoarchitectonic mapping of ten postmortem brains (sample 1 of Table 1) was performed in serial, cell body-stained histological sections as previously described (Zilles et al. 2002b; Amunts et al. 2005).

In short, brains were removed from the skull and fixed for several months in buffered formalin or in Bodian's fixative (pm1 and pm9). The brains were scanned after fixation using magnetic resonance imaging (MRI) (Siemens 1.5-T magnet, Erlanger, Germany) using a T1-weighted three-dimensional (3-D) FLASH sequence (flip angle 40°, repetition time = 40 ms, and echo time = 5 ms for each image), (3-D MRI scan of the fixed brain). The brains were dehydrated in graded alcohols, embedded in paraffin and serially sectioned with a microtome into 20 µm-thick sections. Each 15th section was mounted on a glass slide, stained for cell bodies (Merker 1983) and digitized (the high-resolution flatbed scans of the stained histological section).

Every 15th to 60th section was used for cytoarchitectonic analysis (Fig. 1a, b).

Cytoarchitectonic mapping and nomenclature used

The rostro-caudal extent of the amygdalar subdivisions was manually traced onto high-resolution scans of histological sections in both hemispheres using in-house software (SectionTracer) (Fig. 2). In a refined cytoarchitectonic analysis, we identified ten subdivisions: the anterior amygdaloid area, the amygdalopiriform transition area, the amygdalohippocampal transition area, the basolateral nucleus, basomedial nucleus, the central nucleus, the lateral nucleus, the medial nucleus, paralaminar nucleus and the ventral cortical nucleus. In contrast to our prior cytoarchitectonic study (Amunts et al. 2005), we included the posterior cortical nucleus into the amygdalohippocampal transition area in accord with the latest classification of de Olmos (2004) based on the histochemical data. Furthermore, the posterior cortical nucleus was too small in its in-plane- and rostro-caudal extent for generation of the probabilistic map. Overall, we adopted the nomenclature of de Olmos (2004), except for his anterior cortical nucleus which we did not segregate. We mapped our medial nucleus following the criteria of Brockhaus (1938) for his Area perisupraamygdalaris (psAi, psAv) and Supraamygdaleum superficiale (sAsfi, Asfv). According to assignment of Heimer et al. (1999), both structures (with their parcellations) represent not only the medial nucleus (its superficial and deep part, respectively), but also the anterior cortical nucleus. In addition, segregation of the anterior cortical nucleus from the medial nucleus would lead to a problem in generation of their maps due to decrease in size of the structures (see below, in 'Computation of continuous and maximum probabilistic maps').

Our classification of the subdivisions was originally based on that of Heimer et al. (1999) adopted by Amunts et al. (2005) for the amygdala, but excluding 'Structures topographically related to the amygdala' of Heimer et al. In addition to the laterobasal and superficial groups of the amygdala, 'centromedial group' (instead of 'nuclei of extended amygdala' of Heimer et al.) was segregated on the basis of included subdivisions, i.e., the central and medial nuclei (excluding the bed nuclei of stria terminalis to be a subject of a separate study).

The refined analysis also served the goal of identification and mapping of the internal and related external fiber bundles in the amygdala in the same sections. The identification of fiber bundles was based on their comparison with the micrographs and descriptions published by Brockhaus (1938), as well as on observation of their direction in the myeloarchitectonic sections. However, the single fiber bundles of the internal fiber bundle system are too small to be adequately represented at the relatively low spatial resolution of the anatomical MNI reference space (Evans et al. 2012). Therefore, for computation of the probabilistic maps (see below), the identified fiber masses were merged into two internal fiber structures: (1) the medial fiber bundles [including the intermediate caudomedial fiber masses (icm) and the Lamella medialis (lm) of de Olmos (1990) and Brockhaus (1938)] and (2) the intermediate fiber bundles [including the intermediate central fiber masses (ice), the intermediate orolateral fiber masses (iol) and the Lamellae dorsales (ld) of de Olmos (1990) and Brockhaus (1938)]. The stria terminalis associated with the amygdala represented an external fiber bundle which was mapped in its ventro-medial part (*vtm*, Brockhaus 1938) (Fig. 2).

As compared to the prior study, the classification of the subdivisions into the three major groups is reconsidered here (as result of analysis of the molecular fingerprints, see below).

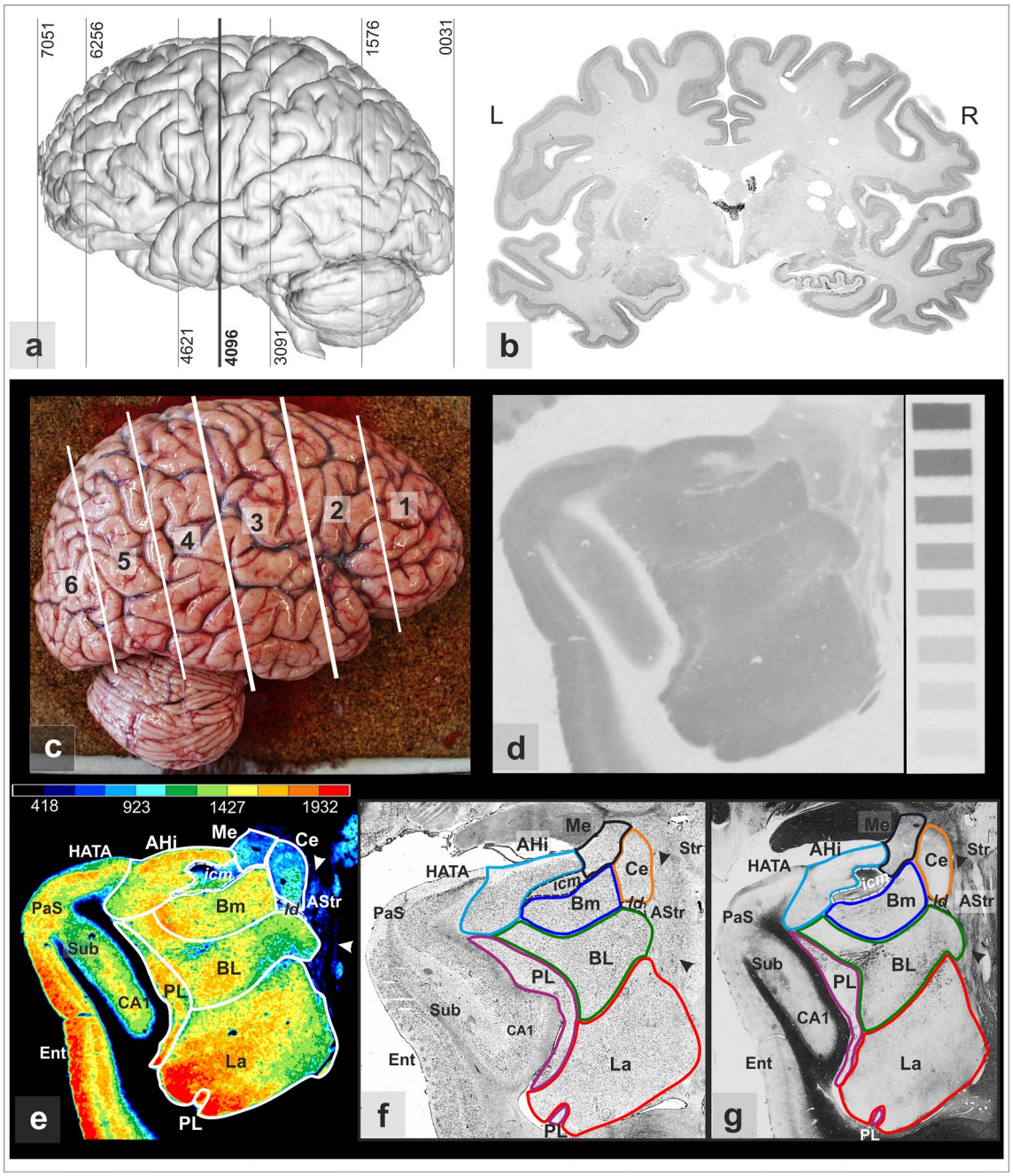

Fig. 1 Cyto- and receptor-architectonic analysis. **a** Postmortem brain (pm8) (3-D reconstruction, left hemisphere) used for cytoarchitectonic mapping; lines with numbers identify approximate positions of coronal sections. **b** Cell body-stained coronal section 4096 with the amygdala (*L* left, *R* right hemisphere). **c** Postmortem brain (rpm1), right hemisphere used for the receptor-architectonic mapping; the brain was cut into six slabs (marked by lines); slab 3 is containing the amygdala. **d** $GABA_B$ receptor autoradiograph together with the co-exposed [^{3}H]-standards, which were used for calculating the correlation of radioactivity concentrations and gray values. **e** $GABA_B$ receptor densities in fmol/mg protein (see color scale above) in various subdivisions of the amygdala. The borders were first identified in cytoarchitectonic (**f**) and myeloarchitectonic (**g**) sections, taken at the approximately same sectioning level. *AHi* amygdalohippocampal transition area, *Bm* basomedial nucleus, *BL* basolateral nucleus, *La* lateral nucleus, *PL* paralaminar nucleus, *Ce* central nucleus, *Me* medial nucleus. Fiber bundles (dashed lines): *icm* intermediate caudomedial fiber masses, *ld* 'Lamellae dorsales' (Brockhaus 1938). Neighboring structures: *AStr* amygdalostriatal transition zone, *Ent* entorhinal cortex, hippocampal formation: *CA1* region I of the Cornu ammonis, *HATA* hippocampal–amygdaloid transition area (Rosene and van Hoesen 1987), *Sub* subiculum proper, *PaS* parasubiculum, *Str* striatum

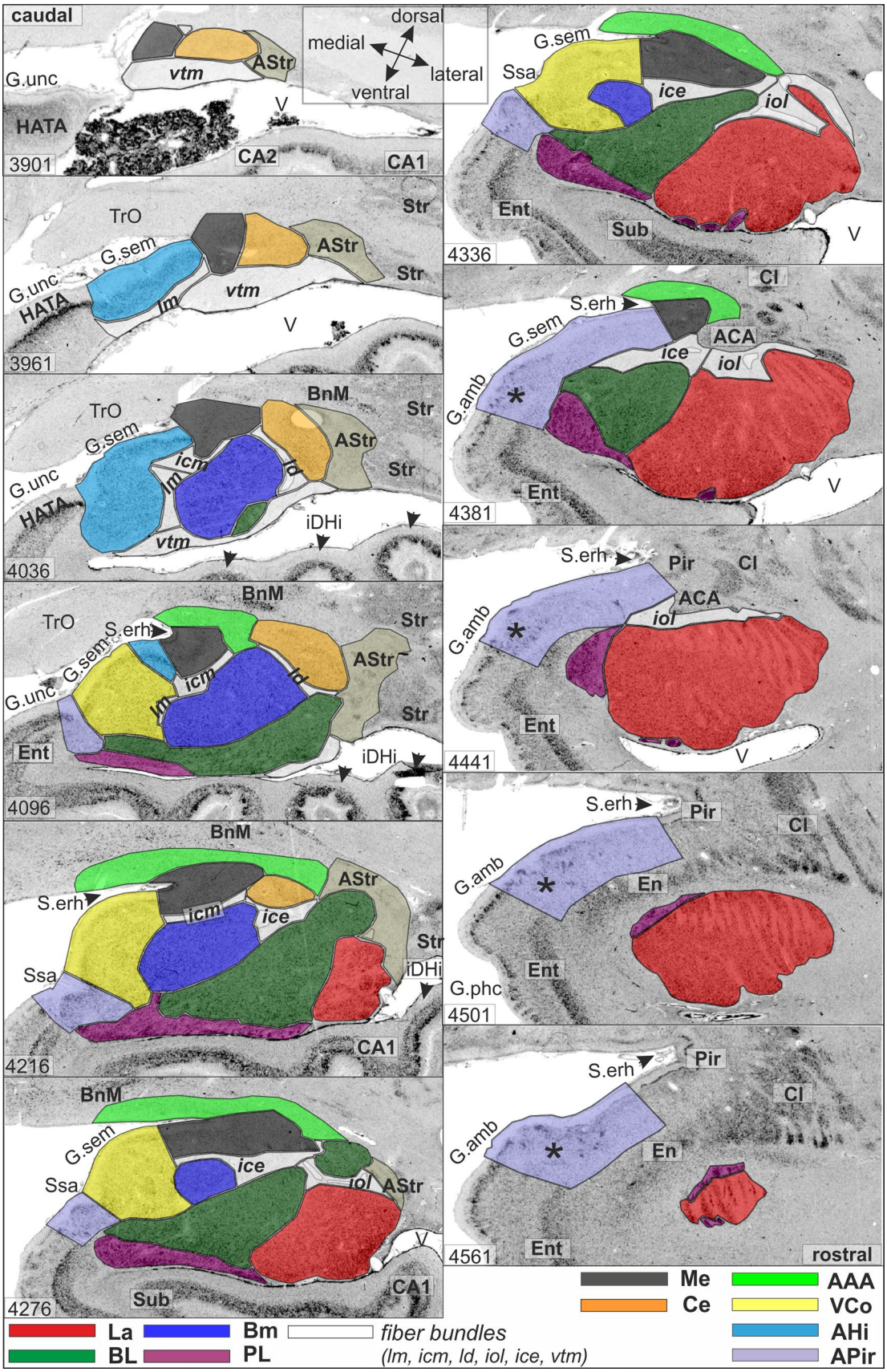

◂**Fig. 2** Sequence of coronal sections illustrating the extent of the subdivisions and fiber bundles from the most caudal to most rostral levels of a right hemisphere. Subdivisions, superficial group: *AAA* anterior amygdaloid area, *AHi* amygdalohippocampal transition area, *APir* amygdalopiriform transition area, *VCo* ventral cortical nucleus; laterobasal group: *Bm* basomedial nucleus, *BL* basolateral nucleus, *La* lateral nucleus, *PL* paralaminar nucleus; centromedial group: *Ce* central nucleus, *Me* medial nucleus (classification of Heimer et al. 1999). Medial fiber bundles: *icm* intermediate caudomedial fiber masses, *lm* 'Lamella medialis' (Brockhaus 1938); intermediate fiber bundles: *ld* 'Lamellae dorsales' (Brockhaus 1938), *ice* intermediate central fiber masses, *iol* intermediate orolateral fiber masses; external fiber bundle *vtm* stria terminalis (ventro-medial part). Asterisks mark a part of *APir* characterized by cell clusters. Neighboring structures of the amygdala: *AStr* amygdalostriatal transition zone, *ACA* amygdaloclaustral transition area, *Cl* Claustrum, *En* endopiriform nucleus, *Ent* entorhinal cortex, *BnM* basal nucleus of Meynert, *Pir* piriform cortex, *Str* striatum, subdivisions of the hippocampal formation: *CA1, CA2* region I and region II of the Cornu ammonis, *HATA* hippocampal–amygdaloid transition area (Rosene and van Hoesen 1987), *Sub* subiculum. Macroanatomical landmarks: *G. amb* Gyrus ambiens, *G. sem* Gyrus semilunaris, *G. phc* Gyrus parahippocampalis, *G. unc* Gyrus uncinatus, *iDHi* Digitationes hippocampi (internal), *S. erh* Sulcus endorhinalis, *Ssa* Sulcus semiannularis, *TrO* Tractus opticus, *V* ventriculus lateralis

Volume measurements

Based on the contours traced in the high-resolution sections (Fig. 2), the area values were extracted (in pixels) for each subdivision in each hemisphere and brain. The volume of subdivision was calculated as a sum of areas ($\sum$Ai) for all evaluated sections multiplied by the pixel size for x and y axes (0.02116 and 0.02116 mm, respectively), thickness of the section (0.020 mm) and spacing between the sections (1.2 mm) as well as shrinkage factor for the respective brain in order to obtain the true values for volume (Amunts et al. 2005). We have analyzed from 7 to 23 sections for all subdivisions in one hemisphere.

The volumes of each subdivision were corrected by the fresh volume to eliminate intersubject variability in brain volume. The corrected volumes were tested for interhemispheric and gender differences with pair-wise permutation tests (Bludau et al. 2014; Eickhoff et al. 2007) and subsequent Bonferroni correction for multiple comparisons.

For each permutation test, the volumes were correspondingly grouped (male/female, left/right) and p values were calculated between the means of these groups. All volume values were randomly re-distributed within two groups under the assumption of label exchangeability; 100,000 iterations of calculation were performed between these groups ($p < 0.05$) (Bludau et al. 2014; Eickhoff et al. 2007).

Computation of continuous and maximum probabilistic maps

The probabilistic maps allow considering an exact topography of architectural details at the macrostructural level of MRI (Amunts et al. 2007; Zilles et al. 2002b; Zilles and Amunts 2010). Due to the advances in the processing pipeline, calculation of the continuous probabilistic maps has become possible; they are characterized by a further improved quality of alignment of the histological data to the in vivo reference brain (Mohlberg et al. 2012).

The three-dimensional (3-D) reconstruction of the brain was based on two data sets obtained during the histological processing (the high-resolution scans of the cytoarchitectonic section (20 µm in-plane/pixel) and 3-D MRI scan of the fixed brain ($1 \times 1 \times 1$ mm) were to combine). The borders were traced in the high-resolution scans of the sections before the 3-D reconstruction in contrast to the prior study (Amunts et al. 2005). The labeling of the brain structures in the high-resolution images of the histological sections increased the spatial resolution of the maps of small subdivisions of the amygdala. In order to adjust for the lower resolution of MRI data set, the high-resolution images of the histological sections with the contour lines were downscaled; a box filter was used, which simultaneously assigned a labeled structure to each point of a downscaled image. A nested combination of linear and nonlinear elastic transformations in 2-D and 3-D (Hömke 2006; Mohlberg et al. 2012) was used for the 3-D reconstruction of the brains with the contour lines, and for their subsequent spatial normalization to the MNI-Colin27 reference space, based on the T1-weighted single-subject template in the MNI space (Evans et al. 2012). The reference space was aligned to the anatomical MNI space by linear transformation in y and z plane to have origin at the anterior commissure (Amunts et al. 2005).

We applied the in-house Software. Our aim was to minimize the interpolation artefacts in order to avoid an over- or under-estimation of each subdivision in the reference space (Mohlberg et al. 2012). However, in case of small and superficially located amygdaloid subdivisions (fine-grained parcellation) a tendency to be 'overestimated' in comparison with histological volumes is still strong due to diverse adjustment, normalization and filtering. To further improve the maps in this respect, we applied here a global normalization over all subdivisions to ensure that the added probability of all subdivisions in each voxel never extends 100%. The subdivisions were superimposed in the reference brain, and the continuous probabilistic maps were calculated. The probabilistic map of each subdivision accounts for interindividual variability by describing for each voxel of a reference space the relative frequency [scaled from 0.0 (=0%) to 1.0

(= 100%) and color-coded], with which this structure was found in a sample.

In addition to the maps of all subdivisions, probabilistic maps of the three major amygdaloid groups were also calculated as a sum of respective subdivisions (see below, in 'Results,' 'Molecular organization of the amygdala'). In the same way, probabilistic maps of the medial and intermediate fiber bundles were calculated as a sum of respective individual fiber masses (see above).

Based on the continuous probabilistic maps, the maximum probability maps (MPMs) were generated as non-overlapping maps of all amygdaloid structures using in-house software. Inclusion of the in-between fiber bundles provided spatial continuity of subdivisions/groups in the MPM of the entire amygdala; each voxel of the reference space was assigned to that structure with the highest probability to be found at this position (Eickhoff et al. 2005). If neighboring nuclei or fiber structures showed equal probabilities in a single voxel, this voxel was assigned to the structure which revealed higher average probability in a neighboring 3 × 3 × 3 voxel cube centered at this particular voxel in question. In the case that no neighboring nuclei or fiber structures were present, a lower threshold value was applied, which was calculated from the average value of the thresholds required to filter those structures with existing neighbors accordingly.

Multimodal receptor mapping

Receptor autoradiography

Different receptors of glutamate, GABA, serotonin, acetylcholine, dopamine and adrenaline (Table 2) were investigated in a sample of six deep-frozen hemispheres of five postmortem human brains (two females, three males; age range 72–79 years, Table 1). The brains were obtained according to legal requirements and came from subjects with no history of neurological or psychiatric disorders. After

Table 2 Overview of neurotransmitter systems, receptors and tritiated ligands used

Transmitter system	Receptor			[^{3}H]-Ligand [concentration][a]	KD value	Pharmacology	Displacer[a] [concentration][a]
Glutamatergic	AMPA		α-Amino-3-hydroxy-5-methyl-4-isoxazolepropionic acid	AMPA [10 nM]	10	Agonist	Quisqualate [10 µM]
	Kainate	Kain		Kainate [9.4 nM]	12	Agonist	SYM 2081 [100 µM]
	NMDA		*N*-Methyl-D-aspartate	MK-801 [3.3 nM]	5	Antagonist	(+) MK-801 [100 µM]
GABAergic	$GABA_A$		γ-Aminobutyric acid (GABA)	Muscimol [7.7 nM]	6	Agonist	GABA [10 µM]
	$GABA_B$			CGP 54626 [2 nM]	1.48	Antagonist	CGP 55845 [100 µM]
	Benzodiazepine binding sites of $GABA_A$ receptors	BZ		Flumazenil [1 nM]	2	Antagonist	Clonazepam [2 µM]
Cholinergic	Muscarinic M_1	M_1		Pirenzepine [1 nM]	3	Antagonist	Pirenzepine [2 µM]
	Muscarinic M_2	M_2		Oxotremorine-M [1.7 nM]	0.8	Agonist	Carbachol [10 µM]
	Muscarinic M_3	M_3		4-DAMP [1 nM]	0.2	Antagonist	Atropine [10 µM]
	Nicotinic $\alpha_4\beta_2$	nic		Epibatidine [0.5 nM]	0.07	Agonist	Nicotine [100 µM]
Serotoninergic	5-HT_{1A}		5-Hydroxy-tryptamine (5-HT)	8-OH-DPAT [1 nM]	2	Agonist	Serotonin [1 µM]
	5-HT_2			Ketanserine [1.14 nM]	0.5	Antagonist	Mianserin [10 µM]
(Nor-)adrenergic	α_1			Prazosin [0.2 nM]	0.2	Antagonist	Phentolamine [10 µM]
	α_2			RX-821002 [1.4 nM]	2.8	Antagonist	Phentolamine [10 µM]
Dopaminergic	D_1			SCH-23390 [1.67 nM]	0.14	Antagonist	SKF 83566 [1 µM]

KD the dissociation constant of the ligand

[a]The concentrations are presented for MR-brains; for rpm brains the concentrations and individual displacers may vary in accord with the standard protocols (Zilles et al. 2002b; Palomero-Gallagher et al. 2009)

removal from the skull, the brains were separated into hemispheres, which were then cut into six coronal slabs (thickness 1.5–3 cm) and deep-frozen at − 40 °C and stored in a deep freezer at − 70 °C (Fig. 1c).

Slabs containing the amygdala were serially sectioned with a large-scale cryostat microtome. The 20-µm-thick coronal sections were subsequently thaw-mounted on glass slides, and immediately adjacent sections were used for quantitative in vitro receptor autoradiography by incubation in different solutions containing specific tritiated ligands for labeling 15 different receptor binding sites according to standard protocols (Zilles et al. 2002b; Palomero-Gallagher et al. 2009). Neighboring sections were stained for cell bodies (Merker 1983) and myelin (Gallyas 1979).

The incubation included three steps: (1) *pre-incubation* to remove endogenous ligands, (2) *main incubation* to label binding sites with a tritiated ligand in presence (non-specific binding) or absence (total binding) of appropriate non-labeled displacers (at µmol concentration) and (3) *final rinsing* to eliminate unbound radioactive ligands and buffer salts. Non-specific binding was less than 5% of the total binding. Therefore, the total binding was considered to be equivalent to the specific binding.

Radioactively labeled sections were co-exposed with plastic [^{3}H]-standards of known, step-wise increasing radioactivity concentrations (Microscales; Amersham, Braunschweig, Germany) against tritium-sensitive films for 8–15 weeks. After developing the films, the labeled sections and co-exposed [^{3}H]-standards were digitized using the AxioCam HRm (ZEISS, Germany) and AxioVision image analyzing systems (ZEISS, Germany) as 8-bit images, with gray values from 0 (black) to 255 (white) and an image size of 2776 × 2080 pixels (Fig. 1d). A nonlinear calibration curve was computed to define the correlation between gray values in the digitized images and radioactivity concentrations of the [^{3}H]-standards. Thus, gray values of the digitized images could be pixelwise linearized and binding sites densities (in fmol/mg protein) could be calculated by using the input parameters (ligand concentration in the incubation solution, dissociation constant K_D of the ligand, equivalent protein weight of the standards, specific radioactivity of the ligand, decays per unit time and radioactivity of the ligand, efficiency of the scintillation counter) (for details see Zilles et al. 2002b; Palomero-Gallagher et al. 2009). The finally resulting gray values were a linear function of the binding site concentration (= linearized receptor autoradiographs, Fig. 1d). Only for visualization purposes, the autoradiographs were color-coded to optimize the contrast in regional receptor distribution patterns (Fig. 1e).

Quantification of the receptor densities in subdivisions of the amygdala

Ten subdivisions were identified in color-coded receptor autoradiographs (Fig. 1e) using cyto- and myeloarchitectonic sections as anatomical reference (Fig. 1f, g).

The receptor densities were analyzed in linearized receptor autoradiographs of the amygdala (Fig. 1d), and subdivisions were traced in each autoradiograph to extract the binding sites densities by comparison with neighboring cell body- and myelin-stained sections. In order to consider the laminar structure of the superficial group and the medial nucleus, we delineated contour lines for the superficial molecular (mol) and deeper cellular (cell) layers.

For each receptor type and hemisphere, pixel values within each closed contour line (area or subdivision) were selected in 2–5 sections, and the mean binding site density (fmol/mg protein, absolute receptor density) was calculated by averaging the pixel values across sections.

Receptor densities of all structures (also those composed of two layers, mol + cell of the superficial group and the medial nucleus) were calculated and averaged across the hemispheres (Table 3). These absolute densities were normalized to the densities across all structures (= 100%), separately for each hemisphere and receptor type (Table 4), in order to make the highly different absolute binding site densities of different receptors more easily comparable at a common scaling.

Receptor fingerprints (Zilles et al. 2002a; Zilles and Amunts 2009) were generated as polar coordinate plots of the normalized means of the 15 analyzed receptors to characterize the multi-receptor balance in each cytoarchitectonic subdivision of the amygdala (Fig. 3).

Hierarchical cluster analysis

Data analysis was performed using in-house R-scripts (R Foundation for Statistical Computing; http://www.r-project.org) mainly based on the R-built-in functions *hclust*() for hierarchical clustering, *k-means*() for k-means clustering and *iso.MDS*() for nonlinear, multidimensional scaling (MDS).

For each subdivision of the amygdala, the normalized mean densities of 15 receptors (in %) were combined into a feature vector. The Euclidean distances between each pair of vectors quantified the degree of dissimilarity between the subdivisions and their multi-receptor balance. A nonlinear, multidimensional scaling (MDS) visualized these dissimilarities in two-dimensions (Fig. 4a). The grouping of the subdivisions into clusters sharing a similar balance of receptors was established using a hierarchical cluster analysis (Ward linkage with Euclidean distances).

The resulting clusters were further validated using a silhouette analysis by assessing the degree of separation

Table 3 Mean ± SD of absolute receptor densities (fmol/mg protein) in the nuclei of the amygdaloid complex

	N	AHi		APir		VCo		AAA[a]		Me		Ce	La	BL	BM	PL
		cell	mol	cell	mol	cell	mol	cell	mol	cell	mol					
AMPA	6	442 ± 266	250 ± 108	398 ± 181	224 ± 48	454 ± 244	221 ± 90	193 ± 132	145 ± 72	219 ± 115	157 ± 67	211 ± 133	234 ± 115	321 ± 188	328 ± 171	401 ± 273
NMDA	6	1193 ± 230	776 ± 149	1098 ± 119	704 ± 161	1272 ± 131	772 ± 184	584 ± 110	455 ± 101	747 ± 114	591 ± 136	716 ± 83	1014 ± 135	1041 ± 110	1130 ± 134	1118 ± 105
Kainate	6	280 ± 87	205 ± 91	381 ± 97	238 ± 72	287 ± 101	177 ± 69	231 ± 85	183 ± 70	233 ± 70	181 ± 60	410 ± 115	177 ± 61	221 ± 64	234 ± 71	278 ± 96
$GABA_A$	6	572 ± 186	448 ± 137	599 ± 268	448 ± 198	631 ± 203	406 ± 123	347 ± 214	289 ± 181	380 ± 206	298 ± 156	326 ± 203	758 ± 371	472 ± 232	554 ± 223	618 ± 229
$GABA_B$	6	1884 ± 246	1574 ± 363	1980 ± 546	1589 ± 442	2233 ± 498	1682 ± 414	1174 ± 284	996 ± 384	1371 ± 224	1128 ± 201	1170 ± 250	1813 ± 474	1733 ± 421	1903 ± 377	1870 ± 585
BZ	5	1498 ± 180	1281 ± 284	1618 ± 198	1359 ± 167	1912 ± 156	1510 ± 178	1188 ± 90	945 ± 156	1301 ± 135	1108 ± 77	1080 ± 58	1749 ± 321	1364 ± 111	1678 ± 126	1762 ± 295
M_1	6	512 ± 296	350 ± 201	583 ± 210	383 ± 157	693 ± 271	438 ± 196	285 ± 127	207 ± 83	325 ± 165	263 ± 130	437 ± 179	532 ± 208	608 ± 237	619 ± 287	725 ± 203
M_2	6	94 ± 19	93 ± 27	131 ± 44	127 ± 36	123 ± 54	118 ± 38	159 ± 43	151 ± 40	108 ± 16	117 ± 20	189 ± 30	96 ± 40	160 ± 46	120 ± 43	141 ± 46
M_3	5	663 ± 322	415 ± 201	730 ± 410	481 ± 274	836 ± 464	483 ± 260	455 ± 236	321 ± 154	468 ± 246	362 ± 186	570 ± 331	594 ± 288	707 ± 373	731 ± 376	825 ± 518
nic	6	36 ± 34	30 ± 23	42 ± 26	39 ± 20	36 ± 24	35 ± 24	47 ± 36	49 ± 36	36 ± 31	35 ± 33	36 ± 30	34 ± 30	37 ± 29	38 ± 31	32 ± 25
α_1	6	525 ± 185	352 ± 137	332 ± 118	289 ± 119	385 ± 128	318 ± 133	303 ± 151	352 ± 174	336 ± 144	298 ± 145	255 ± 127	192 ± 86	198 ± 89	305 ± 122	204 ± 95
α_2	6	303 ± 266	191 ± 181	224 ± 216	165 ± 157	214 ± 189	141 ± 123	224 ± 165	200 ± 125	212 ± 179	173 ± 132	209 ± 170	108 ± 95	150 ± 134	190 ± 169	170 ± 162
$5\text{-}HT_{1A}$	6	389 ± 109	316 ± 64	681 ± 295	437 ± 155	441 ± 163	316 ± 75	119 ± 55	112 ± 36	127 ± 63	107 ± 42	83 ± 47	190 ± 79	317 ± 100	274 ± 98	500 ± 193
$5\text{-}HT_2$	6	306 ± 132	241 ± 118	270 ± 132	211 ± 112	301 ± 131	238 ± 110	250 ± 132	311 ± 163	256 ± 119	246 ± 127	253 ± 122	327 ± 131	278 ± 130	299 ± 128	287 ± 133
D_1	6	54 ± 36	36 ± 25	62 ± 51	42 ± 36	62 ± 56	46 ± 50	59 ± 47	46 ± 45	53 ± 46	44 ± 37	52 ± 47	65 ± 45	70 ± 53	63 ± 55	60 ± 53

BZ benzodiazepine binding sites, *cell* cellular layer, *mol* molecular layer

[a]Sample size was N-1

Table 4 Mean ± SD (%) of normalized receptor densities in the subdivisions of the amygdala, including the layers

	N	AHi		APir		VCo		AAA[a]		Me		Ce	La	BL	BM	PL
		cell	mol	cell	mol	cell	mol	cell	mol	cell	mol					
AMPA	6	137 ± 27	85 ± 29	132 ± 26	82 ± 29	144 ± 14	75 ± 15	61 ± 16	49 ± 16	70 ± 8	52 ± 11	64 ± 10	77 ± 11	102 ± 11	106 ± 9	125 ± 27
NMDA	6	116 ± 16	75 ± 9	107 ± 6	68 ± 9	124 ± 3	75 ± 11	56 ± 7	44 ± 7	73 ± 5	57 ± 8	70 ± 4	99 ± 5	102 ± 2	110 ± 5	110 ± 11
Kainate	6	117 ± 12	83 ± 17	159 ± 11	99 ± 17	118 ± 18	73 ± 20	93 ± 13	75 ± 22	96 ± 8	75 ± 14	173 ± 31	74 ± 16	92 ± 4	97 ± 8	115 ± 12
$GABA_A$	6	102 ± 26	81 ± 28	100 ± 16	75 ± 15	110 ± 24	71 ± 17	50 ± 13	41 ± 13	61 ± 8	48 ± 6	51 ± 11	125 ± 36	77 ± 8	94 ± 11	105 ± 10
$GABA_B$	6	107 ± 12	90 ± 22	110 ± 6	88 ± 15	125 ± 9	94 ± 13	64 ± 4	53 ± 10	77 ± 7	64 ± 7	66 ± 6	101 ± 6	97 ± 5	107 ± 5	103 ± 13
BZ	5	95 ± 12	82 ± 20	102 ± 4	86 ± 11	121 ± 7	96 ± 12	73 ± 4	58 ± 12	82 ± 5	70 ± 4	69 ± 8	110 ± 13	86 ± 3	106 ± 5	111 ± 10
M_1	6	87 ± 22	60 ± 15	108 ± 20	72 ± 22	124 ± 9	78 ± 11	50 ± 8	37 ± 7	57 ± 11	47 ± 11	78 ± 5	95 ± 5	109 ± 3	108 ± 11	135 ± 19
M_2	6	77 ± 9	75 ± 14	103 ± 9	102 ± 23	94 ± 17	94 ± 16	132 ± 34	127 ± 44	89 ± 16	99 ± 35	155 ± 26	74 ± 13	128 ± 13	94 ± 10	111 ± 21
M_3	5	103 ± 14	66 ± 15	109 ± 7	71 ± 7	124 ± 7	73 ± 9	65 ± 3	47 ± 4	71 ± 5	55 ± 5	83 ± 8	91 ± 5	106 ± 3	111 ± 2	119 ± 14
nic	6	95 ± 13	85 ± 13	120 ± 17	120 ± 32	103 ± 13	99 ± 17	123 ± 9	132 ± 14	96 ± 5	92 ± 13	98 ± 8	89 ± 9	102 ± 5	102 ± 7	89 ± 6
α_1	6	209 ± 44	137 ± 21	129 ± 20	109 ± 10	151 ± 19	120 ± 18	112 ± 12	129 ± 16	126 ± 9	110 ± 15	92 ± 19	73 ± 13	74 ± 9	117 ± 9	77 ± 13
α_2	6	181 ± 26	107 ± 27	124 ± 22	94 ± 18	129 ± 15	86 ± 11	130 ± 21	138 ± 76	132 ± 20	123 ± 64	134 ± 19	64 ± 12	89 ± 8	113 ± 7	97 ± 12
$5\text{-}HT_{1A}$	6	137 ± 17	113 ± 22	235 ± 71	151 ± 29	151 ± 16	112 ± 15	41 ± 15	40 ± 11	44 ± 15	39 ± 16	30 ± 15	64 ± 19	108 ± 6	93 ± 10	172 ± 32
$5\text{-}HT_2$	6	104 ± 7	80 ± 14	89 ± 11	69 ± 15	102 ± 8	80 ± 18	75 ± 16	94 ± 23	85 ± 9	80 ± 16	83 ± 8	114 ± 20	92 ± 8	101 ± 3	96 ± 11
D_1	6	90 ± 16	60 ± 14	98 ± 8	65 ± 10	94 ± 13	66 ± 19	88 ± 23	66 ± 30	82 ± 14	69 ± 18	80 ± 21	108 ± 16	113 ± 3	96 ± 15	93 ± 14

Reference for normalization was area-weighted mean through all layers and nuclei of the amygdala (laterobasal, superficial and centromedial groups)

BZ benzodiazepine binding sites, *NA* noradrenaline, *DA* dopamine, *cell* cellular layer, *mol* molecular layer

[a]Sample size was N-1

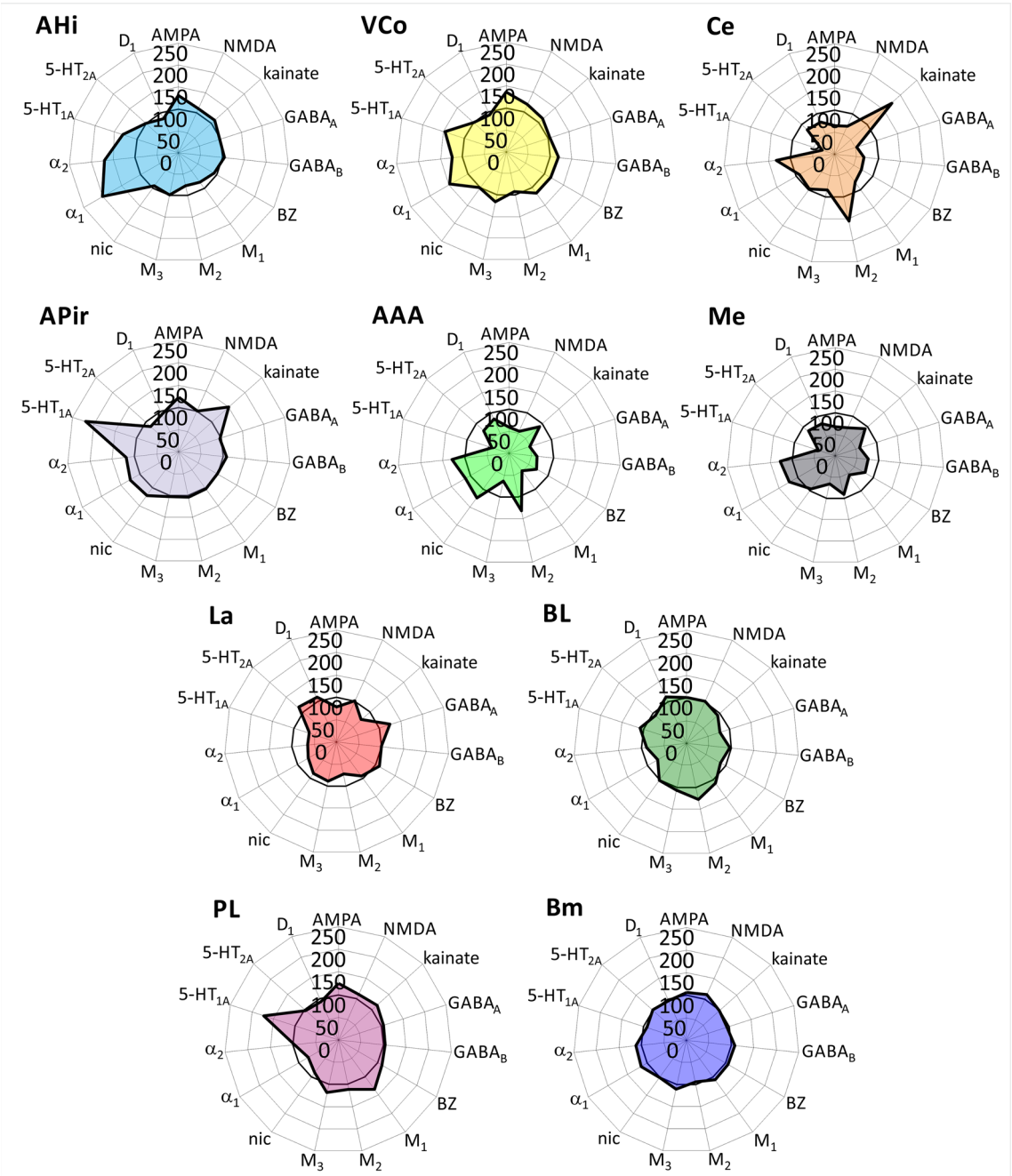

Fig. 3 Receptor fingerprints of the 15 receptor mean densities (in %, based on the data summarized in Table 4, but generated for the entire subdivisions of the amygdala, i.e., mol + cell). For the abbreviations see Fig. 2. In each polar plot, the bold 100% line connects the grand area-weighted means for each receptor

distance between the clusters and the cluster members within a cluster (Fig. 4b). Silhouette widths (SW) were calculated (1) for each cluster solution (two- and three-cluster solutions, Average SW), (2) for each cluster in such a solution (cluster SW), and (3) for each subdivision in each cluster (e.g., PL in the three-cluster solution). In particular, for each subdivision in a cluster the 'within-cluster' dissimilarity with all its neighbors within its cluster and the 'between-cluster' dissimilarity with all data points in the neighboring cluster were calculated (Rousseeuw 1987). Values close to 1 reflect a stable position of a subdivision in its cluster. A zero value indicates the position of a subdivision at the border between two clusters ('intermediate case'), while negative values indicate a subdivision closer to its nearest cluster than to its own ('misclassified case'). The silhouette width of a distinct solution was defined as an average of the silhouette

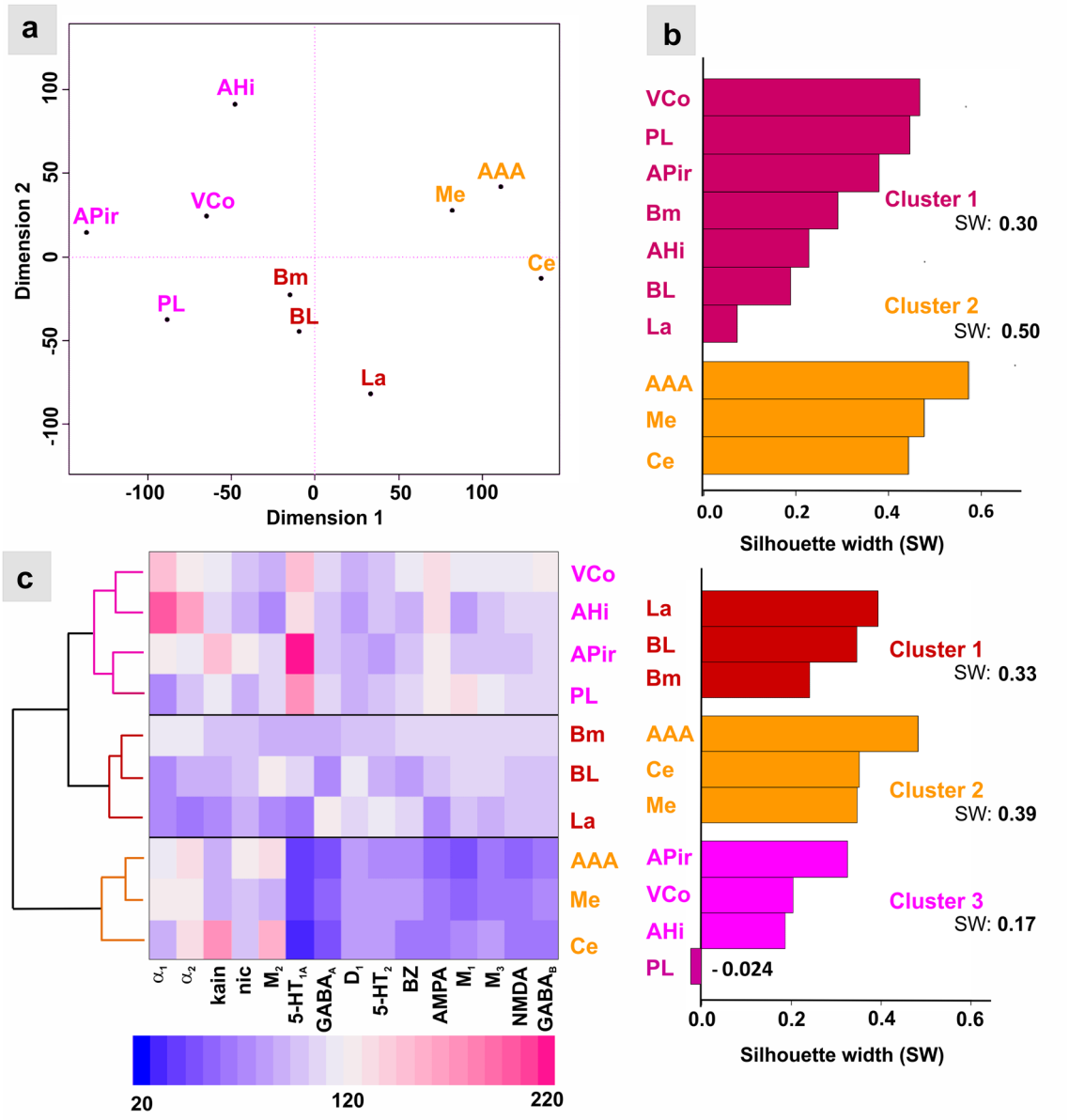

Fig. 4 Receptor-driven clustering of the amygdaloid subdivisions. **a** Multidimensional scaling: each point in the 2-D (Euclidean) space represents a receptor feature vector, reflecting the multi-receptor balance of each subdivision. Abbreviations as in Fig. 2. The smaller the Euclidean distances the higher the similarity between the subdivisions in their receptor-architectonic organization. Three clusters are labeled in red (laterobasal), pink (superficial) and yellow (centromedial), respectively. Note the boundary position of the paralaminar nucleus (PL). **b** Plots of the silhouette values (width) of the two-cluster solution (upper plot) and the three-cluster solution (lower plot). On the y-axis, the subdivisions are organized by decreasing silhouette values in each cluster. In the three-cluster solution, the paralaminar nucleus (PL) has a slightly negative silhouette value, reflecting its unstable cluster assignment. **c** Dendrogram of the hierarchical cluster analysis indicating the three-cluster solution. The heat map shows the densities of the receptors in the different subdivisions according to their classification in one of the three clusters. The color legend codes the normalized receptor densities in % with high values in red and low values in blue colors. While the 5-HT_{1A} receptor (red) contributes to assignment of PL to the superficial amygdala, many other receptors show similarity to the laterobasal amygdala. Note also the high similarity of the anterior amygdaloid areas (AAA) with the medial and central nuclei of the centromedial group

values across the clusters. A *k*-means cluster analysis cross-validated the results of the hierarchical cluster analysis.

To analyze contribution of individual receptors to the grouping of the subdivisions as revealed by the hierarchical cluster analysis, we established a heat map as a color-coded graph of the normalized mean receptor values in a matrix defined by the receptor types and the subdivisions of the amygdala (Fig. 4c).

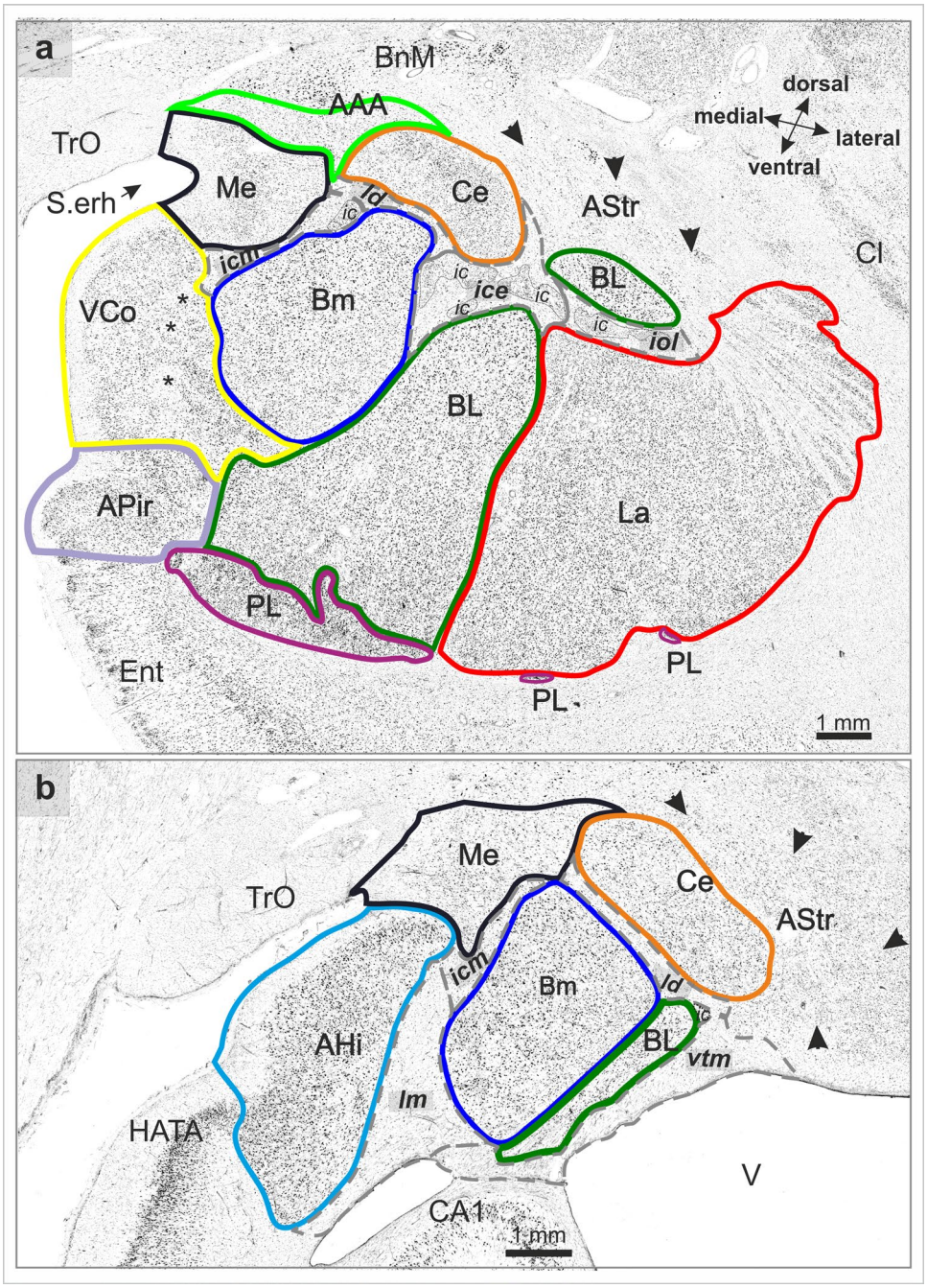

Fig. 5 Cytoarchitecture of the amygdala. Subdivisions of the amygdala delineated at **a** rostral and **b** caudal level. For the abbreviations see Fig. 2. In **a**, asterisks mark the cell-sparse regions of the deep layer of the ventral cortical nucleus. Neighboring structures: *AStr* amygdalostriatal transition zone, *CA1* region I of the Cornu ammonis (hippocampus), *Cl* claustrum, *Ent* entorhinal cortex, *BnM* basal nucleus of Meynert, *HATA* hippocampal-amygdaloid transition area (Rosene and van Hoesen 1987). Macroanatomical features: *S. erh* Sulcus endorhinalis, *TrO* Tractus opticus, *V* Ventriculus lateralis. (**c**) Cytoarchitecture of ten amygdaloid subdivisions and the neighboring structure (*AStr*); colors as in Fig. 2. The asterisk means that APir is here presented at the more anterior level that in **b**, comparable to section 4441–4561 in Fig. 2. In the superficial amygdala and medial nucleus, the black arrows point toward the molecular layer. Blue arrows in the dorsal *VCo* show the fork-shaped cells. The dashed line in *AStr* separates characteristic cell clusters from cell-sparse zones

Results

Cytoarchitecture and topography of amygdaloid subdivisions

Ten subdivisions of the amygdala were identified and mapped (Fig. 5a, b) in their rostro-caudal extent relying on the classical studies (see above, in 'Materials and methods') and are described here using the adopted classification of Heimer et al. 1999 (Amunts et al. 2005). Subdivisions of the superficial group were alike the cortical structures by having both a molecular and a cellular layer. The neurons in the superficial group were of various shapes: from roundish and darkly stained neurons in the amygdalohippocampal transition area to specific fork-shaped neurons in the dorsal part of the ventral cortical nucleus (Fig. 5c). Most neurons of the anterior amygdaloid area were small and spindle-shaped. They were loosely packed and oriented parallel to each other, in particular in the deeper rostral part of the area (Fig. 5c). The rostral portion of the amygdalopiriform

Fig. 5 (continued)

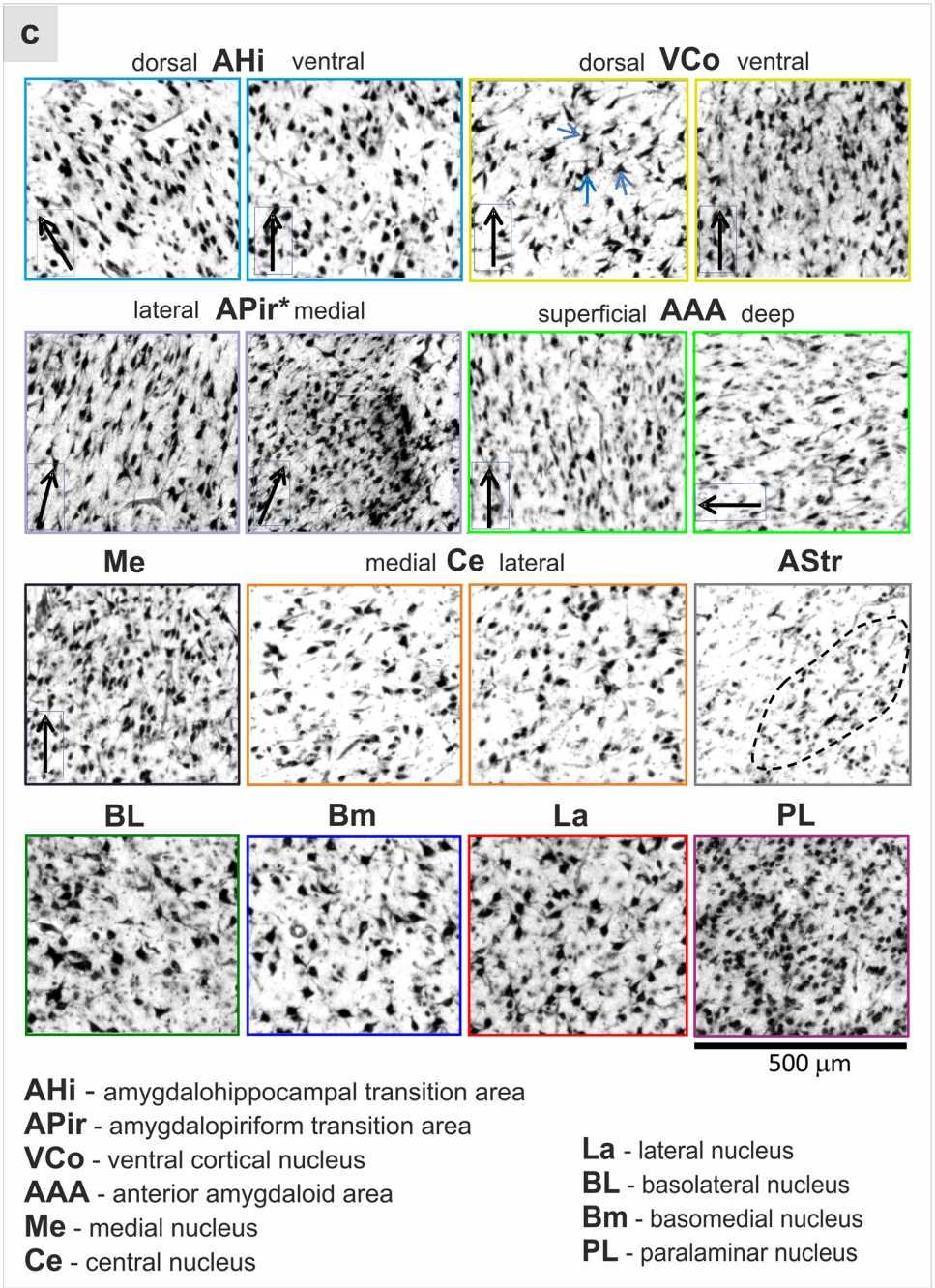

transition area showed most variations in cell arrangement and density, from cell clusters (medial part, Fig. 5c, asterisks in Fig. 2) to loosely located neurons (lateral part, Fig. 5c), as well as in cell shape and size. The centromedial group contained small, mostly lightly stained neurons. Similarly to the superficial group, the medial nucleus had the molecular layer and cellular layer; neurons in the latter were densely packed. The central nucleus contained round, oval and spindle neurons, which were slightly smaller and more densely packed in its lateral part than in the medial part (Fig. 5c). The subdivisions of the laterobasal group had a more compact cell arrangement than the adjacent structures and showed large, medium and small cells (Fig. 5c). The basolateral nucleus (dorsal and dorsolateral parts) contained the largest cells in the amygdala (Fig. 5c). The paralaminar nucleus contained very small, darkly stained and densely packed cells (Fig. 5c).

Some of the subdivisions of the amygdala showed a close topographical relationship to surrounding sulci and gyri and the lateral ventricles (Fig. 2, Table 5). For example, the anterior amygdaloid area was always located at the dorsal lip of the Sulcus endorhinalis . Other subdivisions were not associated with any landmarks, e.g., the basolateral, basomedial

Table 5 Relationship of the subdivisions to gross macroanatomical landmarks

Amygdaloid subdivisions/abbreviations	Localization in a series of coronal sections	Topographical relationship to macroanatomical landmarks (Fig. 2)
Amygdalohippocampal transition area/AHi	Full rostro-caudal extension	At the caudal part of the Gyrus semilunaris
Amygdalopiriform transition area/APir	Rostral part	At the ventral lip of the Sulcus endorhinalis; and at the dorsal part of the Gyrus ambiens (up to rostral limit of APir)
	Caudal part	At the ventral lip of the Sulcus semianularis (up to the caudal limit of APir)
Ventral cortical nucleus/VCo	Full rostro-caudal extension	Occupies the most 'developed' (most curved) part of the Gyrus semilunaris, as compared to more flat appearance of this Gyrus more caudally
Anterior amygdaloid area/AAA	Superficial part	At the dorsal lip of the Sulcus endorhinalis
Medial nucleus/Me	Rostral part	At the fundus of the Sulcus endorhinalis
	Caudal part	At the merging point of the Tractus opticus and Gyrus semilunaris
Central nucleus/Ce		–
Lateral nucleus/La	Except for most rostral parts	Medially adjacent to the rostral extension of the Ventriculus lateralis (temporal horn) for 1.2–7.2 mm
Basolateral nucleus/BL		–
Basomedial nucleus/Bm		–
Paralaminar nucleus/PL	Ventral border	Dorsally adjacent to the obliterated Ventricle and the hippocampal alveus

and central nucleus. However, even if a relationship was found, it did not indicate the precise position of the borders. For example, the temporal horn of the lateral ventricles did not precisely and reliably define the rostral border of the lateral nucleus, which extended beyond the limits of the ventricle for 2.4–6 mm, depending on the hemisphere. The same holds true for the hippocampal alveus, which does not predict the rostral border of the paralaminar nucleus.

The basal nucleus of Meynert and the piriform cortex are located dorsally to the amygdala. Small groups of magnocellular neurons of the former structure (*Ch4 posterior group*, Zaborszky et al. 2008) were adjacent to the anterior amygdaloid area and the centromedial group (Fig. 2). The piriform cortex abuts the amygdalopiriform transition area and was distinguished from the latter by a narrow layer 2 containing very densely packed cells (Stephan 1975). The entorhinal cortex is located ventrally to the amygdalopiriform transition area. The former had a characteristic laminar structure (layers 1–6) and a less wide molecular layer than the amygdalopiriform transition area.

The amygdala also bordered to the transitional areas of the neighboring structures (hippocampus, striatum and claustrum), i.e., to the hippocampal–amygdaloid transition area (Rosene and Van Hoesen 1987), the amygdalostriatal transition zone (de Olmos 2004) and the amygdaloclaustral transition area (de Olmos 2004), respectively (Fig. 2). The hippocampal–amygdaloid transition area was distinguished by a narrower cortex and smaller as well as more densely packed neurons compared to the adjacent amygdalohippocampal transition area (Fig. 5b).

The amygdalostriatal transition zone showed a higher fiber content and a more heterogeneous cell distribution than the medio-ventral subdivisions of the amygdala. It had a few large and darkly stained neurons among masses of small, lightly stained neurons, arranged in small clusters. Loosely packed neurons were found between the clusters (Fig. 5c). The amygdaloclaustral transition area contained cells which were more darkly stained, larger and more densely packed than in the adjacent, medially located amygdaloid subdivisions. The endopiriform nucleus (Heimer et al. 1999; Claustrum praeamygdaleum ventrale of Brockhaus 1938) was separated from amygdalar subdivisions by cell-sparse zones and formed by darkly stained, densely packed cells.

Fiber bundles of the amygdala

The individual fiber masses (*icm, lm; ld, ice, iol; vtm*) separated the amygdaloid subdivisions (Fig. 2). The *icm* underlay the medial nucleus in its caudal aspect (Fig. 5a, b), whereas the ventrally adjacent *lm* separated the amygdalohippocampal transition area from the deeper subdivisions (Fig. 5b). These fibers were united into the *medial fiber bundles* for the generation of the maps (see also above, in 'Materials and methods'). The stria terminalis (*vtm*) also occupied more caudal aspects of the amygdala (at the level of the amygdalohippocampal transition area, Figs. 2, 5b). It was distinguished from the medially situated *lm* by preferred diagonal orientation of fibers in the former.

The thin fiber bundle of *ld* separated the central and basomedial nuclei (Fig. 5a, b). It merged rostrally into the fiber

Table 6 Volumes of the subdivisions grouped by hemispheres (unadjusted) mean ± standard deviation (SD), CV—coefficient of variation, = SD/mean

$N=10$	Left (mm^3)	CV	Right (mm^3)	CV	p
AHi	49 ± 23	0.46	53 ± 19	0.36	0.61
APir	169 ± 35	0.21	196 ± 60	0.31	0.04**
VCo	127 ± 35	0.21	123 ± 28	0.23	0.46
AAA	97 ± 25	0.26	99 ± 40	0.41	0.80
Me	93 ± 30	0.33	90 ± 26	0.29	0.39
Ce	53 ± 10	0.19	50 ± 9	0.18	0.44
La	443 ± 70	0.16	449 ± 54	0.12	0.59
BL	270 ± 36	0.13	264 ± 51	0.19	0.45
Bm	134 ± 21	0.16	128 ± 19	0.15	0.15
PL	77 ± 17	0.22	80 ± 12	0.15	0.28
Total mm^3	1512 ± 189		1531 ± 202		

**$p < 0.05$ without Bonferroni correction

masses of *ice* which overlay the basomedial nucleus, and most rostrally also the basolateral nucleus (Figs. 2, 5a). The *ice* merged laterally into the fiber masses of *iol*. The latter fibers were located dorso(-medially) to the amygdala; between its lateral nucleus and the transitional zones to the striatum and claustrum (Figs. 2, 5a). These fiber masses were united into the intermediate fiber bundles.

Intersubject variability in volume

The total volume of the amygdala (both hemispheres), estimated as the sum of all subdivisions, was 3044 ± 381 mm^3 (Table 6). The amygdalohippocampal transition area and the central nucleus were the smallest subdivisions (total volumes: 102 ± 36 and 103 ± 17 mm^3, respectively). The lateral nucleus showed the largest volume (total volume: 892 ± 120 mm^3; Table 6). The permutation test showed significant interhemispheric difference in the corrected volumes of the amygdalopiriform transition area ($p < 0.05$, not corrected for multiple comparisons, Table 6). Its volume in the right hemisphere was larger by a factor of 1.4 than its left-hemispheric counterpart. However, the p value did not reach significance ($p < 0.05$) after the Bonferroni correction for multiple comparisons.

The total volume of the amygdala was 1657 ± 177 mm^3 in male and 1385 ± 65 mm^3 in female brains (left hemispheres: 1650 ± 159 mm^3 in males and 1374 ± 85 mm^3 in females; right hemispheres: 1665 ± 212 mm^3 in males and 1397 ± 44 mm^3 in females). The volume of each subdivision in males showed a tendency to be larger than that in females, but the permutation test did not reveal significant sex differences for the corrected volumes of both the total amygdala and any of its subdivisions ($p > 0.05$). No significant interactions between both hemispheres and gender were found.

Intersubject variability of subdivisions

Probability maps visualize the intersubject variability of the subdivisions in space and extent (Fig. 6a). The lateral nucleus was the only subdivision, which revealed voxels with a 100% overlap, thus indicating the lowest variability among all subdivisions. Variability of the amygdalopiriform transition area and the ventral cortical nucleus was also low (Fig. 6a). The laterobasal group, composed of the lateral, basolateral, basomedial and paralaminar nuclei (Table 7), showed the highest overlap among the three major groups (Fig. 6b). The paralaminar nucleus was included into this summary map considering its close topographical relationship and similarity in receptor pattern, except the serotonergic 5-HT_{1A} receptor (see below, and Fig. 4c). Figure 7 demonstrates the maximum probability maps for the three amygdaloid groups (Fig. 7a) and the amygdaloid subdivisions (Fig. 7b, c) with in-between fiber bundles [medial, intermediate fiber bundles and stria terminalis (vtm)].

Receptors reveal the amygdaloid subdivisions

The cytoarchitectonically defined subdivisions of the amygdala were used as a basis to analyze the receptor architecture of the amygdala (Figs. 8a–s, 9a–l; Tables 3, 4).

The amygdalohippocampal transition area reveals the highest α_1 and α_2 receptor densities of the amygdala (Fig. 8p, s; Tables 3, 4). The amygdalopiriform transition area had the highest 5-HT_{1A} receptor density (Fig. 9c; Tables 3, 4). The border of the ventral cortical nucleus with the medial nucleus was marked by higher cholinergic (except for M_2) and glutamatergic receptors (Fig. 8), as well as serotoninergic and GABAergic receptors (Fig. 9) in this nucleus. Densities of α_1 and 5-HT_{1A} receptors were higher in the ventral cortical nucleus than in the adjacent basomedial nucleus (Figs. 8o, 9c). M_2, $\alpha_4\beta_2$ nicotinic, α_1 and α_2 receptors in the anterior amygdaloid area showed higher densities than in the neighboring basomedial nucleus (Fig. 8i, m, o, r). The central nucleus had the highest kainate receptor densities (Fig. 8f; Table 4). Its border with the basomedial nucleus was clearly marked by M_2 receptors. Their density was lower in the basomedial than in the central nucleus (Fig. 8j). The medial nucleus showed relatively low densities of the receptors (Figs. 8, 9); only its border with the anterior amygdaloid area was marked by the higher densities of benzodiazepine binding sites and $GABA_B$ receptors in the medial nucleus (Fig. 9i, k). Lower M_1, M_3 and higher α_1 receptor densities in the

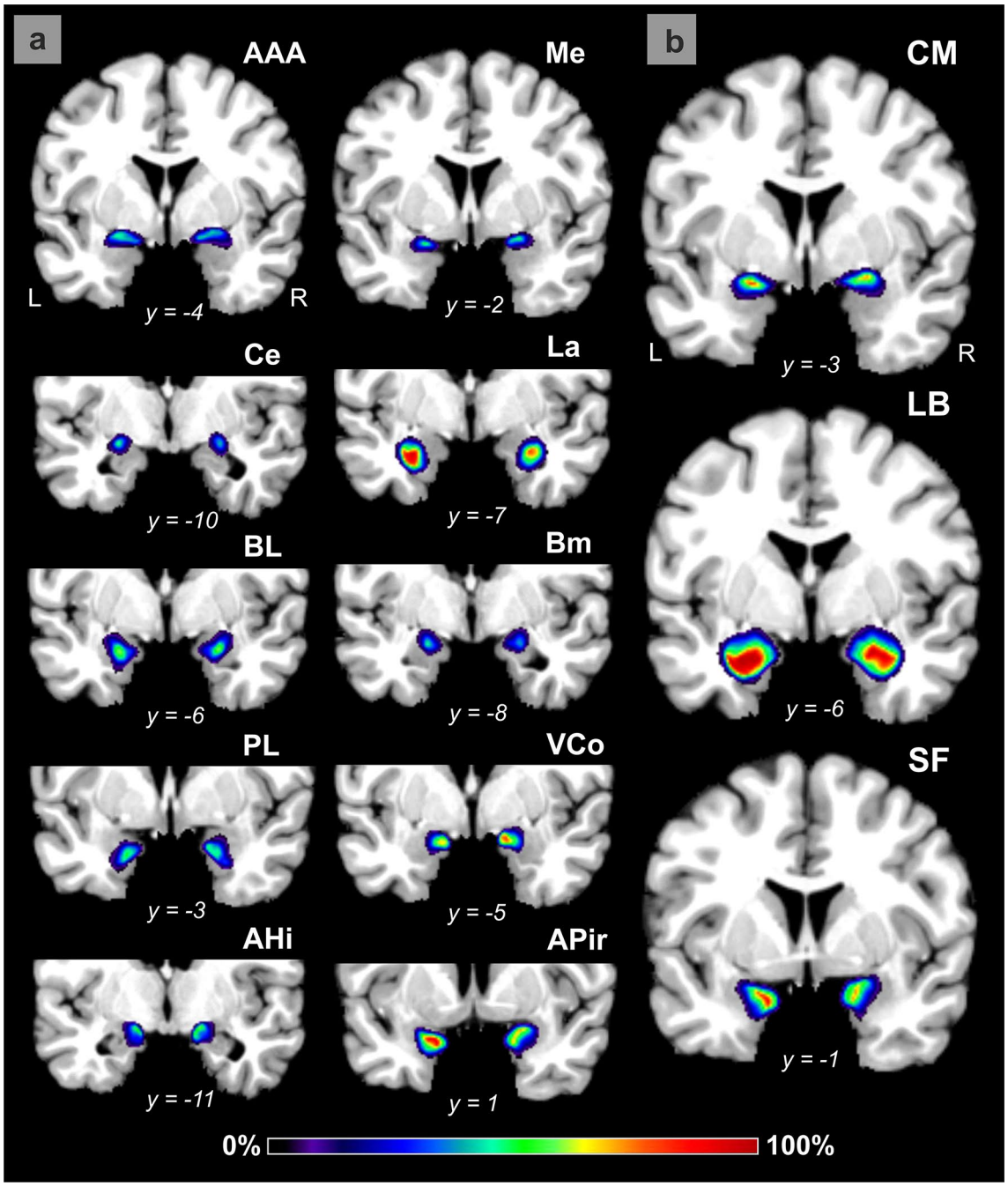

Fig. 6 Probabilistic maps of amygdaloid subdivisions (**a**) and groups (**b**) in the format of the single-subject template of the anatomical MNI space (Amunts et al. 2005; Evans et al. 2012). Abbreviations of the subdivisions as in Fig. 2. *CM* centromedial group of the amygdala, *LB* laterobasal group, *SF* superficial group (the groups include an updated summary of the subdivisions, see 'Results,' 'Molecular organization of the amygdala'). Color bar encodes the probabilities with 100% indicating full overlap, and 0% indicating no overlap of brains in a particular position of the space

medial nucleus marked its border with the central nucleus (Fig. 8h, l, p).

The lateral nucleus displayed the highest $GABA_A$ receptor density in the amygdala (Tables 4, 5). The basolateral nucleus showed higher M_2 and lower $GABA_A$ receptors and benzodiazepine binding sites as compared to the lateral nucleus (Figs. 8i, 9g, i). The basomedial nucleus had higher α_1 receptor densities than the basolateral nucleus (Fig. 8o, p). The paralaminar nucleus was demarcated by the highest densities of M_1 receptors in the amygdala (Fig. 8g; Tables 4,

Table 7 Overview of subdivisions and their assignment to the groups

Classification	Amygdaloid subdivisions	Abbreviations
Amygdaloid subdivisions		
Superficial group	Amygdalohippocampal transition area	AHi
	Amygdalopiriform transition area	APir
	Ventral cortical nucleus	VCo
Centromedial group	Anterior amygdaloid area	AAA
	Medial nucleus	Me
	Central nucleus	Ce
Laterobasal group	Lateral nucleus	La
	Basolateral nucleus	BL
	Basomedial nucleus	Bm
	Paralaminar nucleus	PL[a]

[a]The paralaminar nucleus was classified as being part of the superficial group in the hierarchical cluster analysis, but has a unique position between this and the laterobasal group; to achieve consistency with previous studies, and considering the topography of this nucleus, it has been included into the probabilistic cytoarchitectonic map of the laterobasal group (see text)

5). It also had higher 5-HT_{1A} receptor densities than the dorsally adjacent nuclei (Fig. 9c; Tables 4, 5). Its border with the basolateral nucleus was clearly delineable by the higher AMPA, kainate (Fig. 8a, e), M_1, M_3 (Fig. 8g, k), and benzodiazepine binding site densities (Fig. 9i) in the paralaminar nucleus.

Not all receptors were sensitive to a particular border, but merge several neighboring structures with nearly similar receptor concentration: e.g., the anterior amygdaloid nucleus, the medial and central nuclei showed uniformly low 5-HT_{1A} receptor densities (Fig. 9c, d). M_2 receptor distributions were similar in the central and basolateral nuclei (Fig. 8j). The same was true for the AMPA, NMDA and M_1 receptors, which did not differ between the basomedial and basolateral nuclei (Fig. 8a–d, g, h). The basolateral and paralaminar nuclei showed similar densities of α_1 and 5-HT_2 receptors (Figs. 8o, 9e). The ventral cortical and basomedial nuclei revealed uniform distribution of M_2, D_1 and $GABA_A$ receptors (Figs. 8i, 9a, g). The $\alpha_4\beta_2$ nicotinic receptor was homogeneously distributed throughout the amygdala (Fig. 8m, n). The borders between the subdivisions coincided with changes in the cyto- and myeloarchitectonic pattern, if the receptor type was sensitive to a particular border.

Receptor heterogeneity within amygdaloid subdivisions

The 5-HT_{1A} receptor was heterogeneously distributed in the amygdalohippocampal transition area, suggesting a further subdivision into a dorsal (lowest density), an intermediate and a ventral (highest density) part (Fig. 9d, see arrows). The ventral part also showed the highest kainate receptor densities (Fig. 8f, see an arrow). In the central nucleus, higher kainate, M_2, M_3, α_1 and 5-HT_2 receptors receptor densities separated a lateral part (Figs. 8f, j, l, p, 9f), and higher AMPA, α_2 receptors and benzodiazepine binding sites were found in its medial part (Figs. 8a, s, 9j). In the *lateral nucleus*, lower densities of AMPA, NMDA, M_1, M_3, α_1, 5-HT_2 and $GABA_B$ receptors characterized its dorsolateral part (dashed line in Figs. 8a, c, g, k, o, 9e, k). Higher NMDA, $GABA_A$ and $GABA_B$ receptor densities indicated a ventro-lateral part (dashed line in Figs. 8c, 9g, k). The ventro-medial part of the lateral nucleus was clearly separated by lower densities of $GABA_A$ and benzodiazepine receptor binding sites (Fig. 9g, i). In the *basomedial nucleus*, α_1 and α_2 receptor densities were higher caudally than rostrally (Fig. 8o, p, r, s). Higher caudal than rostral densities were found for M_2 and 5-HT_{1A} receptors in the basolateral nucleus (Figs. 8i, j, 9c, d). In addition, the dorso-lateral part of the basolateral nucleus revealed higher M_2 receptors (Fig. 8i) and lower AMPA, NMDA, M_1, M_3 and $GABA_B$ receptor densities than the more ventral part (Figs. 8a, c, g, k, 9k). The ventral part of the basolateral nucleus was also marked by higher 5-HT_{1A} receptors and benzodiazepine binding sites (Fig. 9c, i).

Molecular organization of the amygdala

Receptor fingerprints visualize similarities and dissimilarities between amygdaloid subdivisions and reflect the balance between the densities of multiple receptor types (Fig. 3). The fingerprints of the lateral, basolateral and basomedial nuclei were highly similar in shape (Fig. 3). The same was true for the comparison between the anterior amygdaloid area and the medial nucleus. In contrast, the paralaminar nucleus, the amygdalopiriform transition area, the central nucleus and amygdalohippocampal transition area have distinguishing fingerprint patterns.

The hierarchical cluster analysis further analyzed receptor similarities. It offered two solutions, which were nearly identical.

The two-cluster solution combined the anterior amygdaloid area, the medial and central nuclei into one cluster (cluster of an ‘extended’ centromedial group) and the remaining subdivisions into a second cluster. The three-cluster solution (Fig. 4a, b) resulted in: (1) a cluster combining subdivisions of the laterobasal group (lateral, basolateral and basomedial nuclei), (2) a cluster with the subdivisions of the superficial group (ventral cortical nucleus, amygdalopiriform and amygdalohippocampal transition areas) and the paralaminar nucleus and (3) a cluster of the ‘extended’ centromedial group as in the previous solution.

In order to provide arguments favouring one or the other solution, we applied a silhouette analysis, which estimates

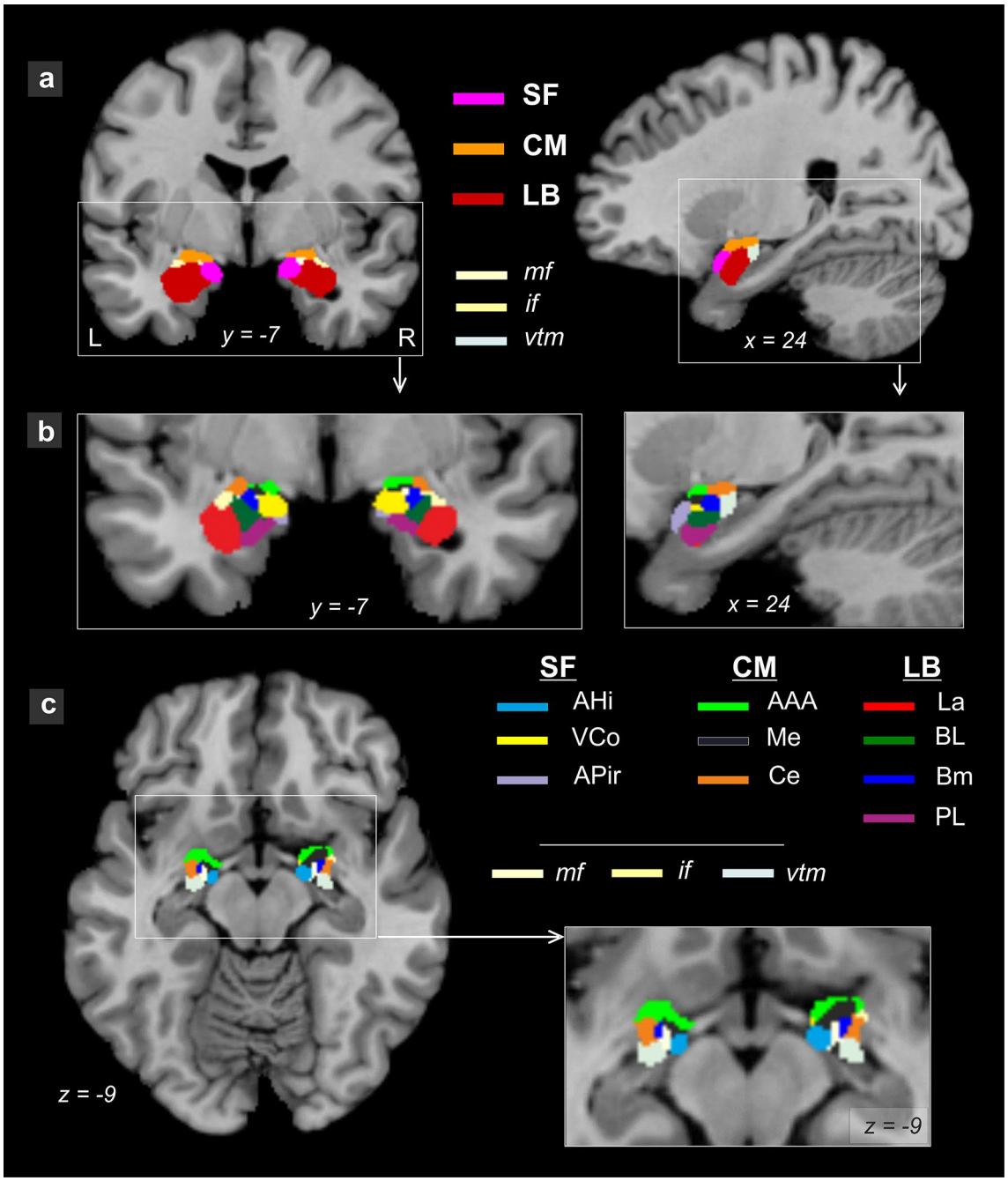

Fig. 7 Non-overlapping, maximum probability maps (MPM) of the human amygdala. **a** MPMs of the three amygdaloid groups and in-between fibers in a coronal (left) and sagittal (right) section in the anatomical MNI reference space. *CM* centromedial group, *LB* laterobasal group, *SF* superficial group (an assignment of the subdivisions into the groups is updated, as compared to Amunts et al. 2005), *mf* medial fiber bundles, *if* intermediate fiber bundles, *vtm* ventro-medial part of stria terminalis, *L* left hemisphere, *R* right hemisphere. **b** MPM of amygdaloid subdivisions and in-between fibers at the same levels as in **a. c** MPM of the amygdaloid subdivisions and fibers in a horizontal section at $z = -9$. For the abbreviations of the amygdaloid subdivisions and fibers see Fig. 2

the stability of the clusters and respective solutions (Fig. 4b). It revealed an unstable assignment of the parala-minar nucleus within its cluster as indicated by a negative SW (SW = − 0.024; Fig. 4b); this value reduced the overall stability of the cluster (SW = 0.17), i.e., this nucleus could also be associated to another group, which is supported by its position in the two-dimensional scaling (Fig. 4a). In order to analyze the impact of the individual receptor types to this

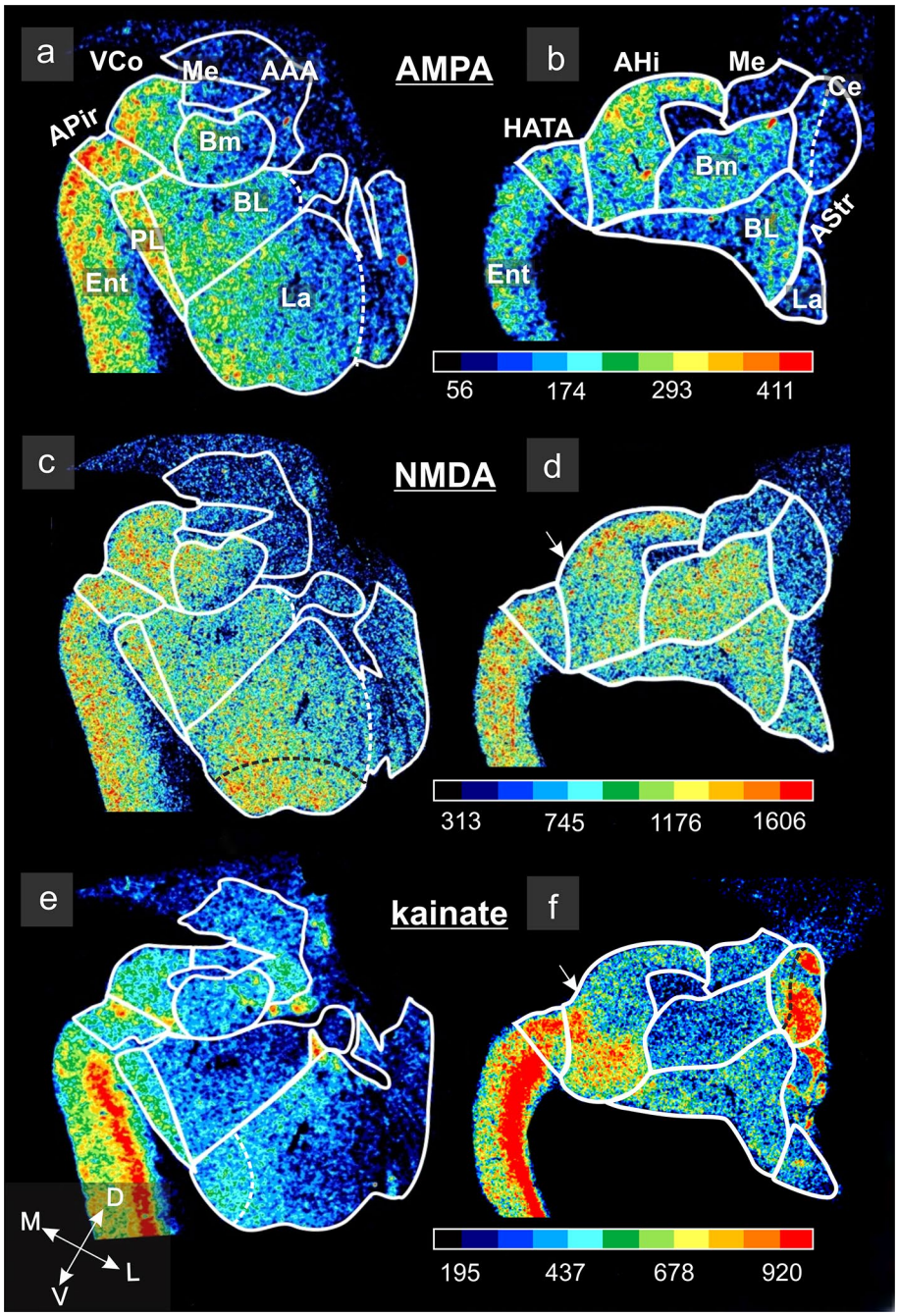

Fig. 8 Distribution of receptors in the rostral (**a, c, e**) and caudal (**b, d, f**) amygdala, visualized in glutamatergic AMPA, NMDA and kainate receptor autoradiographs. The autoradiographs of different neurotransmitter receptors are immediately adjacent to each other for both rostral and caudal levels. The dashed lines within some of the subdivisions define some of its sub-parcellations based on the receptor architecture (dorso-lateral part of *BL, La*; ventro-medial and dorsomedial parts of *La*; subdivisions of *Ce*). The arrows mark the ventral part of *AHi*. Abbreviations of the amygdaloid subdivisions (see in Fig. 2), relevant for all glutamatergic autoradiographs, are marked on AMPA receptor autoradiograph. Adjacent structures: *Ent* entorhinal cortex, *HATA* hippocampal–amygdaloid transition area (Rosene and van Hoesen 1987). Color scales code the concentrations for each receptor, indicated in fmol/mg protein. *D* dorsal, *V* ventral, *M* medial, *L* lateral. Distribution of receptors in the rostral (**g, i, k**) and caudal (**h, j, l**) amygdala, visualized in cholinergic M_1, M_2 and M_3 receptor autoradiographs. The sub-parcellations (e.g., dorsal and dorso-lateral parts of *BL*; dorso-lateral and ventro-lateral part of *La*; subdivisions of *Ce*) are marked by dashed lines. Abbreviations of the amygdaloid subdivisions, relevant for all cholinergic autoradiographs, are marked on M_1 receptor autoradiograph. Distribution of receptors in the rostral (**m, o, r**) and caudal (**n, p, s**) amygdala, visualized in cholinergic nicotinic, and adrenergic α_1 and α_2 receptor autoradiographs. The dashed lines within *Me* and *Ce* nuclei define their fine receptor-based subparcellations. Abbreviations of the amygdaloid subdivisions, marked on nicotinic receptor autoradiograph, are relevant for the other autoradiographs

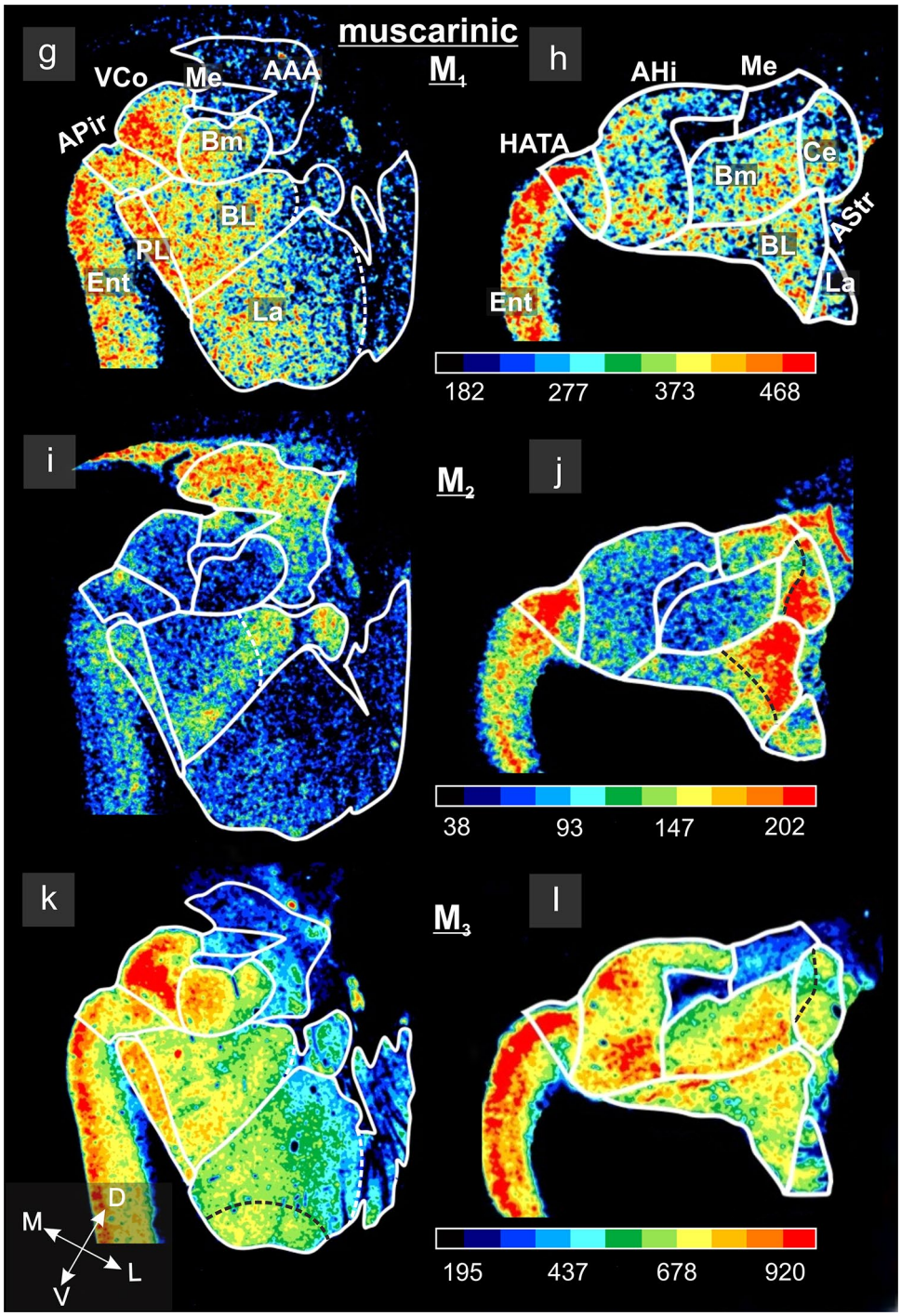

Fig. 8 (continued)

result, a heat map with all receptor types and subdivisions was generated (Fig. 4c). For example, high kainate and M_2 receptors (red colors in the heat map) distinguished the central nucleus from the remaining subdivisions of the centromedial amygdala. High adrenergic α_1 receptors combine the ventral cortical nucleus and amygdalohippocampal transition area. The heat map revealed that the anterior amygdaloid area was similar to the medial nucleus in, e.g., α_1 receptor expression, and to both medial and central nuclei in α_2 and 5-HT_{1A} receptors (Fig. 4c); therefore, the anterior amygdaloid area was assigned, as a consequence, to the centromedial group (Table 7).

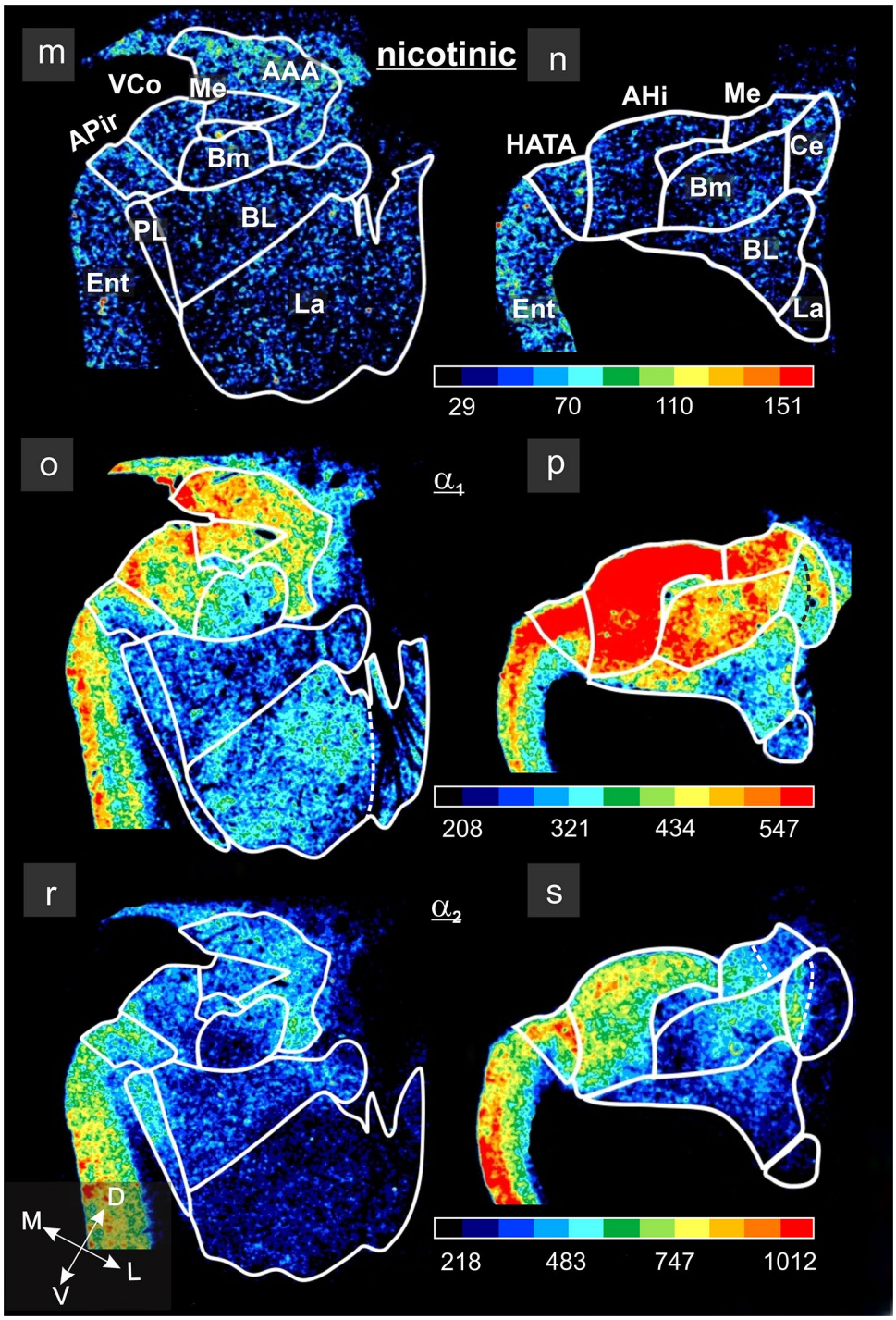

Fig. 8 (continued)

Interestingly, the ambiguous position of the paralaminar nucleus in its clustering was shown mainly due to the 5-HT_{1A} receptor density (indicated by red color): the high value was similar to that of the amygdalopiriform transition area and was the major reason for associating the paralaminar nucleus to the superficial amygdala (Fig. 4c).

The discussion of the principles of the molecular organization of the amygdala is thus based on

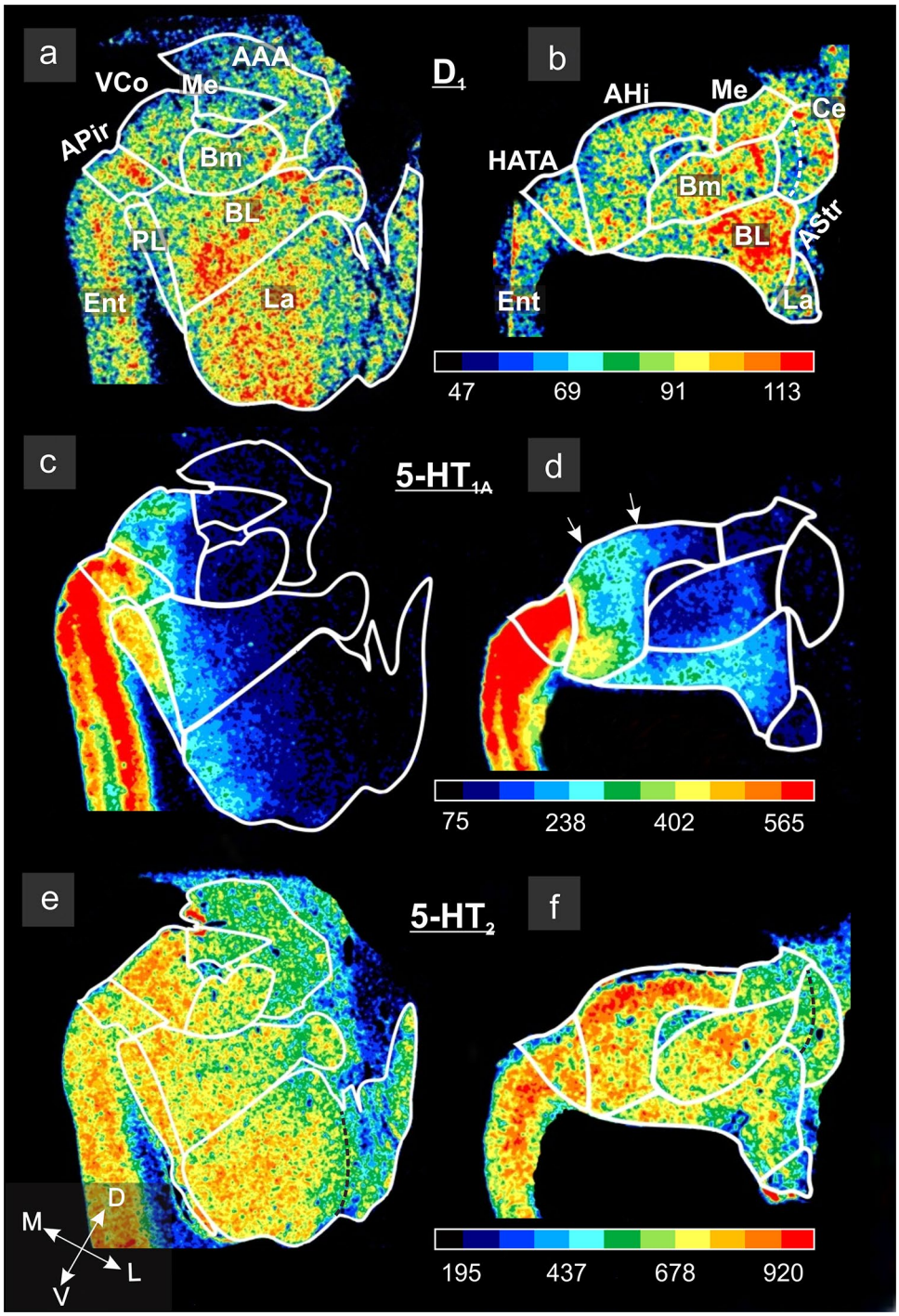

Fig. 9 Distribution of receptors in the rostral (**a, c, e**) and caudal (**b, d, f**) amygdala, visualized in dopaminergic D_1, serotoninergic 5-HT_{1A} and 5-HT_2 receptor autoradiographs. The dashed lines define the dorsolateral part of *La* and parts of *Ce*. In 5-HT_{1A} receptor autoradiograph, arrows mark a possible tripartition of *AHi*. Abbreviations of the amygdaloid subdivisions, relevant for the other autoradiographs, are designated on D_1 receptor autoradiograph. Distribution of receptors in the rostral (**g, i, k**) and caudal (**h, j, l**) amygdala, visualized in GABAergic $GABA_A$, benzodiazepine (BZ) and $GABA_B$ binding site autoradiographs. The dashed lines within the lateral nucleus define some of its receptor-architectonic subparcellations. Abbreviations of the subdivisions, relevant for all GABAergic receptor autoradiographs, are designated for $GABA_A$ receptor

both (two- and three-) cluster solutions (see details in 'Discussion').

Discussion

In the current study, we analyzed the organization of the amygdala with focus on its various subdivisions which show distinct connectivities and functions in animal studies (Holland and Gallagher 1999; LeDoux 2000; LaLumiere 2014; McGaugh 2002; Stefanacci and Amaral 2002). The cytoarchitectonic fine-grained parcellation of the human amygdala into ten subdivisions is the basis for the volumetric measurements, mapping and the receptor analyses. The subdivisions are components of major amygdaloid groups. Our previous cytoarchitectonic parcellation into the lateral, centromedial and superficial groups relied on the classification of Heimer et al. (1999). This previous study of our group

Fig. 9 (continued)

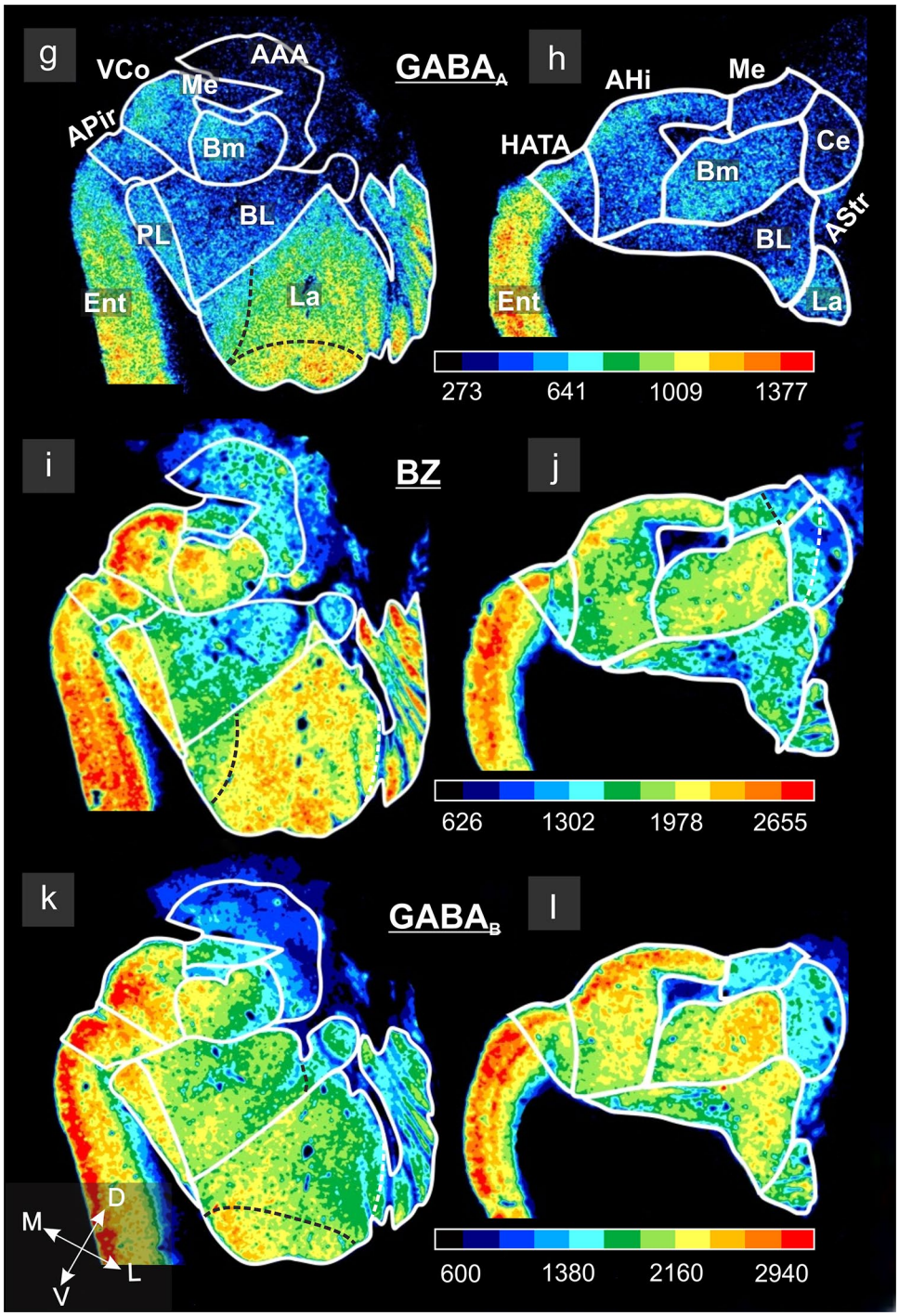

presented for the first time probabilistic maps of these major groups which have been successfully used as an anatomical basis for functional imaging studies, e.g., the fMRI study of Koelsch et al. (2013) showed responsivity of the bilateral superficial group of the amygdala and auditory cortex to music, with signal intensity which increased during joy and decreased during fear. A later study found that the 'small-world' network underlying joy can be extended to the laterobasal group of the amygdala (Koelsch and Skouras 2014). Here, we offer the fine-grained probabilistic maps, based on state-of-the-art 3D-reconstruction and image processing, as a prerequisite for an anatomically precise localization of functional imaging data for future functional studies implicating the subdivisions of the human amygdala. It is especially intriguing to segregate functions of the subdivisions of the superficial amygdala, which were overlooked in the animal studies but seem to play an important role in socially relevant functions (also Goossens et al. 2009).

In the focus of the study, we addressed the organization of the amygdala on multiple levels: the amygdala is not only a cytoarchitectonically, but also chemoarchitectonically heterogeneous brain structure regarding distribution of different neurotransmitter receptors. The principles behind this interplay of function, molecular and cellular architecture are still not well understood, especially in humans. It has been previously shown that the lateral, the basomedial and the central nuclei are separate sites of plasticity in fear learning (Amano et al. 2011; Blair et al. 2001; Keifer et al. 2015; LeDoux 2000). In both the lateral and basolateral nuclei, Pape and Stork (2003) demonstrated selective expression of molecular factors (genes) related to GABA function during fear conditioning, supporting the view of these nuclei as sites of plasticity. In humans, the probabilistically mapped laterobasal amygdaloid group was reported as a site of increased fear processing in conditions of induced noradrenergic neurotransmission by the noradrenaline-reuptake inhibitor reboxetine, as compared to the placebo baseline, in the pharmacological fMRI study using the facial emotion paradigm (Onur et al. 2009). The enhanced noradrenaline signaling in the laterobasal group was suggested to be a crucial factor contributing to etiology of post-traumatic stress disorder (Onur et al. 2009).

Involvement of the basolateral nucleus in memory processing was dependent on cholinergic (Power et al. 2003), GABAergic (Castellano et al. 1989), adrenergic (Ferry et al. 1999) and serotoninergic (Bombardi and Di Giovanni 2013) neurotransmission, as well as on interaction of neurotransmitter systems (Pare 2003; Rezayof et al. 2011). Modulatory influences of glutamatergic, dopaminergic, serotoninergic, noradrenergic and cholinergic neurotransmission on the inhibitory tonus (GABAergic regulation) allow keeping an exquisite balance in the network activity of the basolateral nucleus (Prager et al. 2016).

In addition to processing of fearful information and memory consolidation, the same nucleus was functionally involved in different functions, e.g., in acquisition and representation of reinforcement value by implicating different external connections in animal studies (Holland and Gallagher 1999).

The fingerprint demonstrates the balance of multiple receptors (excitatory, inhibitory and modulatory) which are involved in all relevant functions of a subdivision. Specific shape and size of the fingerprints may thus indicate functional specialization of the subdivisions. On the other hand, a degree of similarity of the fingerprints to each other leads to their functionally relevant grouping. To address question of classification of the amygdaloid subdivisions (a model of amygdalar organization), we covered multiple aspects of amygdalar organization (in contrast to focusing on one single modality) and used an approach which is based on quantitative data and statistical procedures. Based on a hierarchical cluster analysis we were seeking to build a hierarchy of subdivisions, and to achieve a biologically motivated parcellation of subdivisions considering molecular fingerprints. Such approach has been proven successful in the past for several cortical areas, e.g., the cingulate (Palomero-Gallagher et al. 2009), and the visual cortex (Eickhoff et al. 2008), inferior parietal lobe (Caspers et al. 2013) and Broca's region (Amunts et al. 2010; Zilles et al. 2015).

Our hierarchical cluster analysis of different receptor fingerprints related to the different subdivisions revealed two solutions with two and three clusters, respectively. However, it was not possible to decide which cluster number would be superior based on this analysis alone. In the literature, both two- (e.g., Johnston 1923; McDonald 2003) and three-cluster solutions were reported (e.g., Amunts et al. 2005; Nieuwenhuys et al. 2008; Heimer et al. 1999 for comparison).

In the two-cluster solution, the central, medial nuclei and anterior amygdaloid area formed one group, while all other subdivisions built a second group. The two clusters include phylogenetically old, 'extended centromedial' part (subpallial, extended amygdala) and new (pallial amygdala) part consisting of the superficial (cortical) and laterobasal groups ('corticobasolateral amygdala,' McDonald 2003), respectively.

Another two-cluster solution comes from neuroimaging, revealing a superior (medial) and an inferior (lateral) cluster based on connectivity-driven approach (Bach et al. 2011; Mishra et al. 2014). However, the quality of their clusters was different: the superior (medial) cluster combined the superficial and centromedial amygdaloid groups, while the inferior (lateral) cluster included the laterobasal group.

In the three-cluster solution, the group containing the central, medial nucleus and the anterior amygdaloid area was the same as in the two-cluster solution, but the second, large cluster was further split into a group (1) containing the lateral nucleus, the basolateral nucleus and the basomedial nucleus on the one hand, and (2) the amygdalopiriform area, the ventral cortical nucleus, the amygdalohippocampal transition area and the paralaminar nucleus, on the other. These clusters largely coincided with those described in our previous study (Amunts et al. 2005) and were further supported by a recent connectivity-driven parcellation (Bzdok et al. 2013). The latter authors showed the best correspondence of their clusters, based on the brain-wide co-activation maps with the cytoarchitectonically defined amygdaloid groups (Fig. 3 of Bzdok et al. 2013) as compared to the other imaging studies.

The subdivisions were further evaluated using a silhouette analysis. Silhouette values were calculated as measure of how stable an association of a certain subdivision to a cluster is. As a result of the additional analysis of the hot map, the three-cluster solution was chosen. Moreover, new light was shed onto two subdivisions:

First, the analysis indicated the intermediate position of the paralaminar nucleus between the superficial and laterobasal groups. Although the paralaminar nucleus showed a high similarity of 5-HT_{1A} receptors to the amygdalopiriform transition area and other subdivisions of the superficial group, the pattern of other receptor types was more similar to the laterobasal group. The negative silhouette values of the paralaminar nucleus (grouped together with amygdalopiriform area, the ventral cortical nucleus, and the amygdalohippocampal transition area into one cluster) indicates that this classification is not stable. Our data therefore provide evidence of a unique role of the paralaminar nucleus, which agrees with arguments of the other studies (deCampo and Fudge 2012).

Secondly, in both solutions, the anterior amygdaloid area was more similar to the central and medial nucleus as compared to all other subdivisions. It was therefore attributed to the centromedial group, in contrast to previous research (Amunts et al. 2005). All its subdivisions showed a medium level of α_1 and α_2 densities, and very low concentrations of 5-HT_{1A} receptors. This is in contrast to the superficial group, which showed high densities of α_1 and α_2 as well as 5-HT_{1A} receptors. Developmental studies seem to support this result: the ventral part of the anterior amygdaloid area showed a common origin with components of the medial nucleus (anterior peduncular area, as revealed by *Lhx6* gene expression), whereas the dorsal part of the anterior amygdaloid area had a striatal origin similarly to the central nucleus (lateral ganglionic eminence, as revealed by *Dlx5* and *Lmo4* expression) (García-López et al. 2008).

It has been shown that the noradrenergic and serotoninergic neurotransmitter systems are affected by social stress and anxiety (Fuchs and Flugge 2003). A pharmacological fMRI study examined responses of the healthy subjects to social-emotional stimuli under enhanced levels of noradrenaline (by the noradrenaline-reuptake inhibitor reboxetine), cortisol (by hydrocortisone) or both (Kukolja et al. 2008). This study reported a decreased activation of the amygdala to positive stimuli, but an increase in the amygdala activation to negative stimuli in a latter condition. The authors found that the cytoarchitectonically defined centromedial and superficial groups were most sensitive to the combined action of these two neuromodulators. This finding agrees with our receptor data as reflected by fingerprints and the hot map: subdivisions of the centromedial and superficial group showed high densities of α_1 and α_2 receptors.

Within the superficial group, the receptor fingerprints of the medial nucleus and the anterior amygdaloid area [which constituted 'temporal lobe components of the medial extended amygdala' of de Olmos (2004)] were most similar, while the central nucleus differed from both. This finding corroborates a distinction between the medial and central nuclei described in relation to their different origin and molecular, gene-related profiles (García-López et al. 2008): the medial nucleus contained cell groups of diverse subpallial, non-striatal origin (as revealed by *Lhx6, Shh* gene expression) and some groups of pallial origin (*Lhx9* gene expression for the ventral pallium) in contrast to the uniform striatal origin of the central nucleus. Distinct gene expression profiles in specific embryonic divisions correlated with dissociated functional pathways of the medial and central nuclei, which were involved in defensive/reproductive behavior and fear/anxiety, respectively (Martínez-García et al. 2008).

Conclusions

The current study provides a detailed receptor-architectonic characterization of multiple receptor types in the human amygdala and its cytoarchitectonic subdivisions. The latter open a way to link the microstructure of the brain to its function, dysfunction and finally behavior. Moreover, the multimodal approach allowed proposing criteria for a parcellation of the amygdala, based on quantitative markers of the molecular architecture. A unique position of the paralaminar nucleus was defined based on receptor data, which was classified as part of the superficial group based on a high signal of 5-HT_{1A} receptors, although other receptor types are more similar to the laterobasal group. The anterior amygdaloid area was classified as part of the centromedial group, while in the past it was usually associated to the superficial group. Thus, multi-level analyses based on a combination of receptor and cytoarchitectonic mapping contribute to a more comprehensive understanding of the organizational principles of the amygdala (Table 7), opening a way to parcellate structures beyond morphological similarities.

Acknowlegdments We would like to thank Markus Cremer, Sabine Wilms, Stephanie Krause, Angelika Börner, Jessica Teske-Bausch and René Hübbers for their excellent technical assistance.

Compliance with ethical standards

Funding This project has received funding from the European Union's Horizon 2020 Framework Programme for Research and Innovation under Grant Agreement No 720270 (Human Brain Project SGA1).

References

Adolphs R (2010) What does the amygdala contribute to social cognition? Ann N Y Acad Sci 1191:42–61. https://doi.org/10.1111/j.1749-6632.2010.05445.x

Amano T, Duvarci S, Popa D, Pare D (2011) The fear circuit revisited: contributions of the basal amygdala nuclei to conditioned fear. J Neurosci 31:15481–15489. https://doi.org/10.1523/JNEUROSCI.3410-11.2011

Amaral DG, Price JL, Pitkänen A, Carmichael ST (1992) The amygdala: neurobiological aspects of emotion, memory, and mental dysfunction. Wiley, Oxford, pp 1–66

Amunts K, Kedo O, Kindler M, Pieperhoff P, Mohlberg H, Shah NJ, Habel U, Schneider F, Zilles K (2005) Cytoarchitectonic mapping of the human amygdala, hippocampal region and entorhinal cortex: intersubject variability and probability maps. Anat Embryol (Berl) 210:343–352. https://doi.org/10.1007/s00429-005-0025-5

Amunts K, Schleicher A, Zilles K (2007) Cytoarchitecture of the cerebral cortex—more than localization. Neuroimage 37:1061–1065. https://doi.org/10.1016/j.neuroimage.2007.02.037

Amunts K, Lenzen M, Friederici AD, Schleicher A, Morosan P, Palomero-Gallagher N, Zilles K (2010) Broca's region: novel organizational principles and multiple receptor mapping. PLoS Biol 8(9). https://doi.org/10.1371/journal.pbio.1000489

Bach DR, Behrens TE, Garrido L, Weiskopf N, Dolan RJ (2011) Deep and superficial amygdala nuclei projections revealed in vivo by probabilistic tractography. J Neurosci 31:618–623. https://doi.org/10.1523/JNEUROSCI.2744-10.2011

Ball T, Rahm B, Eickhoff SB, Schulze-Bonhage A, Speck O, Mutschler I (2007) Response properties of human amygdala subregions: evidence based on functional MRI combined with probabilistic anatomical maps. PLoS One 2(3):e307. https://doi.org/10.1371/journal.pone.0000307

Benzing WC, Mufson EJ, Jennes L, Stopa EG, Armstrong DM (1992) Distribution of neurotensin immunoreactivity within the human amygdaloid complex: a comparison with acetylcholinesterase- and Nissl-stained tissue sections. J Comp Neurol 317:283–297. https://doi.org/10.1002/cne.903170306

Blair HT, Schafe GE, Bauer EP, Rodrigues SM, LeDoux JE (2001) Synaptic plasticity in the lateral amygdala: a cellular hypothesis of fear conditioning. Learn Mem 8:229–242. https://doi.org/10.1101/lm.30901

Bludau S, Eickhoff SB, Mohlberg H, Caspers S, Laird AR, Fox PT, Schleicher A, Zilles K, Amunts K (2014) Cytoarchitecture, probability maps and functions of the human frontal pole. Neuroimage 93 Pt 2:260–275. https://doi.org/10.1016/j.neuroimage.2013.05.052

Bombardi C, Di Giovanni G (2013) Functional anatomy of 5-HT2A receptors in the amygdala and hippocampal complex: relevance to memory functions. Exp Brain Res 230:427–439. https://doi.org/10.1007/s00221-013-3512-6

Brockhaus H (1938) Zur normalen und pathologischen Anatomie des Mandelkerngebietes. J Psychol Neurol 49:1–136

Bzdok D, Laird AR, Zilles K, Fox PT, Eickhoff SB (2013) An investigation of the structural, connectional, and functional subspecialization in the human amygdala. Hum Brain Mapp 34(12):3247–3266. https://doi.org/10.1002/hbm.22138

Canessa N, Crespi C, Motterlini M, Baud-Bovy G, Chierchia G, Pantaleo G, Tettamanti M, Cappa SF (2013) The functional and structural neural basis of individual differences in loss aversion. J Neurosci 33:14307–14317. https://doi.org/10.1523/JNEUROSCI.0497-13.2013

Caspers S, Schleicher A, Bacha-Trams M, Palomero-Gallagher N, Amunts K, Zilles K (2013) Organization of the human inferior parietal lobule based on receptor architectonics. Cereb Cortex 23:615–628. https://doi.org/10.1093/cercor/bhs048

Castellano C, Brioni JD, Nagahara AH, McGaugh JL (1989) Post-training systemic and intra-amygdala administration of the GABA-B agonist baclofen impairs retention. Behav Neural Biol 52:170–179

Cortés R, Probst A, Palacios JM (1987) Quantitative light microscopic autoradiographic localization of cholinergic muscarinic receptors in the human brain: forebrain. Neuroscience 20:65–107

de Olmos JS (1990) Amygdala. In: Paxinos G (ed) The human nervous system. Academic Press Inc, San Diego, pp 583–710

de Olmos JS (2004) Amygdala. In: Paxinos G, Mai JK (eds) The human nervous system, 2 edn. Elsevier, San Diego, pp 739–868

deCampo DM, Fudge JL (2012) Where and what is the paralaminar nucleus? A review on a unique and frequently overlooked area of the primate amygdala. Neurosci Biobehav Rev 36:520–535. https://doi.org/10.1016/j.neubiorev.2011.08.007

Eickhoff SB, Stephan KE, Mohlberg H, Grefkes C, Fink GR, Amunts K, Zilles K (2005) A new SPM toolbox for combining probabilistic cytoarchitectonic maps and functional imaging data. Neuroimage 25:1325–1335. https://doi.org/10.1016/j.neuroimage.2004.12.034

Eickhoff SB, Schleicher A, Scheperjans F, Palomero-Gallagher N, Zilles K (2007) Analysis of neurotransmitter receptor distribution patterns in the cerebral cortex. Neuroimage 34:1317–1330. https://doi.org/10.1016/j.neuroimage.2006.11.016

Eickhoff SB, Rottschy C, Kujovic M, Palomero-Gallagher N, Zilles K (2008) Organizational principles of human visual cortex revealed by receptor mapping. Cereb Cortex 18:2637–2645

Evans AC, Janke AL, Collins DL, Baillet S (2012) Brain templates and atlases. Neuroimage 62:911–922. https://doi.org/10.1016/j.neuroimage.2012.01.024

Ferry B, Roozendaal B, McGaugh JL (1999) Involvement of alpha1-adrenoceptors in the basolateral amygdala in modulation of memory storage. Eur J Pharmacol 372:9–16

Fruhholz S, Grandjean D (2013) Amygdala subregions differentially respond and rapidly adapt to threatening voices. Cortex 49:1394–1403. https://doi.org/10.1016/j.cortex.2012.08.003

Fuchs E, Flugge G (2003) Chronic social stress: effects on limbic brain structures. Physiol Behav 79:417–427

Fudge JL, Tucker T (2009) Amygdala projections to central amygdaloid nucleus subdivisions and transition zones in the primate. Neuroscience 159:819–841. https://doi.org/10.1016/j.neuroscience.2009.01.013

Gallyas F (1979) Silver staining of myelin by means of physical development. Neurol Res 1:203–209

García-López M, Abellan A, Legaz I, Rubenstein JL, Puelles L, Medina L (2008) Histogenetic compartments of the mouse centromedial and extended amygdala based on gene expression patterns during development. J Comp Neurol 506:46–74. https://doi.org/10.1002/cne.21524

Goossens L, Kukolja J, Onur OA, Fink GR, Maier W, Griez E, Schruers K, Hurlemann R (2009) Selective processing of social stimuli in the superficial amygdala. Hum Brain Mapp 30:3332–3338. https://doi.org/10.1002/hbm.20755

Guarraci FA, Frohardt RJ, Kapp BS (1999) Amygdaloid D1 dopamine receptor involvement in Pavlovian fear conditioning. Brain Res 827:28–40

Heimer L, de Olmos JS, Alheid GF, Pearson J, Sakamoto N, Shinoda K, Marksteiner J, Switzer RC (1999) The Basal Forebrain. Part II. In: Bloom FE, Björklund A, Hökfelt T (eds) Primate nervous system. Part III. Elsevier, Amsterdam, pp 57–226

Hesse E, Mikulan E, Decety J, Sigman M, Garcia MC, Silva W, Ciraolo C, Vaucheret E, Baglivo F, Huepe D, Lopez V, Manes F, Bekinschtein TA, Ibanez A (2016) Early detection of intentional harm in the human amygdala. Brain 139:54–61. https://doi.org/10.1093/brain/awv336

Holland PC, Gallagher M (1999) Amygdala circuitry in attentional and representational processes. Trends Cogn Sci 3:65–73

Hömke L (2006) A multigrid method for anisotropic PDEs in elastic image registration. Numer Linear Algebra Appl 13:215–229

Hurlemann R, Rehme AK, Diessel M, Kukolja J, Maier W, Walter H, Cohen MX (2008) Segregating intra-amygdalar responses to dynamic facial emotion with cytoarchitectonic maximum probability maps. J Neurosci Methods 172:13–20

Hurlemann R, Schlaepfer TE, Matusch A, Reich H, Shah NJ, Zilles K, Maier W, Bauer A (2009) Reduced 5-HT(2A) receptor signaling following selective bilateral amygdala damage. Soc Cogn Affect Neurosci 4:79–84. https://doi.org/10.1093/scan/nsn039

Johnston JB (1923) Further contributions to the study of the evolution of the forebrain. J Comp Neurol 35:337–481

Kalin NH, Shelton SE, Davidson RJ (2004) The role of the central nucleus of the amygdala in mediating fear and anxiety in the primate. J Neurosci 24:5506–5515. https://doi.org/10.1523/JNEUROSCI.0292-04.2004

Keifer OP Jr, Hurt RC, Ressler KJ, Marvar PJ (2015) The physiology of fear: reconceptualizing the role of the central amygdala in fear learning. Physiology (Bethesda) 30:389–401

Klumpers F, Morgan B, Terburg D, Stein DJ, van Honk J (2015) Impaired acquisition of classically conditioned fear-potentiated startle reflexes in humans with focal bilateral basolateral amygdala damage. Soc Cogn Affect Neurosci 10:1161–1168. https://doi.org/10.1093/scan/nsu164

Koelsch S, Skouras S (2014) Functional centrality of amygdala, striatum and hypothalamus in a "small-world" network underlying joy: an fMRI study with music. Hum Brain Mapp 35:3485–3498

Koelsch S, Skouras S, Fritz T, Herrera P, Bonhage C, Kussner MB, Jacobs AM (2013) The roles of superficial amygdala and auditory cortex in music-evoked fear and joy. Neuroimage 81:49–60. https://doi.org/10.1016/j.neuroimage.2013.05.008

Kukolja J, Schlapfer TE, Keysers C, Klingmuller D, Maier W, Fink GR, Hurlemann R (2008) Modeling a negative response bias in the human amygdala by noradrenergic-glucocorticoid interactions. J Neurosci 28:12868–12876. https://doi.org/10.1523/JNEUROSCI.3592-08.2008

LaLumiere RT (2014) Optogenetic dissection of amygdala functioning. Front Behav Neurosci 8(107):1–7. https://doi.org/10.3389/fnbeh.2014.00107

LeDoux JE (2000) Emotion circuits in the brain. Annu Rev Neurosci 23:155–184. https://doi.org/10.1146/annurev.neuro.23.1.155

Martínez-García F, Novejarque A, Lanuza E (2008) Two interconnected functional systems in the amygdala of amniote vertebrates. Brain Res Bull 75:206–213. https://doi.org/10.1016/j.brainresbull.2007.10.019

McDonald AJ (2003) Is there an amygdala and how far does it extend? An anatomical perspective. Ann N Y Acad Sci 985:1–21

McGaugh JL (2002) Memory consolidation and the amygdala: a systems perspective. Trends Neurosci 25:456

Merker B (1983) Silver staining of cell bodies by means of physical development. J Neurosci Methods 9:235–241

Mishra A, Rogers BP, Chen LM, Gore JC (2014) Functional connectivity-based parcellation of amygdala using self-organized mapping: a data driven approach. Hum Brain Mapp 35:1247–1260. https://doi.org/10.1002/hbm.22249

Mohlberg H, Eickhoff S, Schleicher A, Zilles K, Amunts K (2012) A new processing pipeline and release of cytoarchitectonic probabilistic maps—JuBrain. OHBM 2012, Peking, China (Poster)

Niehoff DL, Whitehouse PJ (1983) Multiple benzodiazepine receptors: autoradiographic localization in normal human amygdala. Brain Res 276:237–245

Nieuvenhuys R, Voogd J, van Huijzen C (2008) Telencephalon: amygdala and claustrum. In: The human central nervous system, 4th edn. Springer, pp 401–426

Olsson A, Phelps EA (2007) Social learning of fear. Nat Neurosci 10:1095–1102. https://doi.org/10.1038/nn1968

Onur OA, Walter H, Schlaepfer TE, Rehme AK, Schmidt C, Keysers C, Maier W, Hurlemann R (2009) Noradrenergic enhancement of amygdala responses to fear. Soc Cogn Affect Neurosci 4:119–126. https://doi.org/10.1093/scan/nsn049

Palomero-Gallagher N, Vogt BA, Schleicher A, Mayberg HS, Zilles K (2009) Receptor architecture of human cingulate cortex: evaluation of the four-region neurobiological model. Hum Brain Mapp 30:2336–2355

Pape HC, Stork O (2003) Genes and mechanisms in the amygdala involved in the formation of fear memory. Ann N Y Acad Sci 985:92–105

Pare D (2003) Role of the basolateral amygdala in memory consolidation. Prog Neurobiol 70:409–420

Pazos A, Probst A, Palacios JM (1987a) Serotonin receptors in the human brain-III. Autoradiographic mapping of serotonin-1 receptors. Neuroscience 21:97–122

Pazos A, Probst A, Palacios JM (1987b) Serotonin receptors in the human brain-IV. Autoradiographic mapping of serotonin-2 receptors. Neuroscience 21:123–139

Power AE, McIntyre CK, Litmanovich A, McGaugh JL (2003) Cholinergic modulation of memory in the basolateral amygdala involves activation of both m1 and m2 receptors. Behav Pharmacol 14:207–213. https://doi.org/10.1097/01.fbp.0000073702.15098.21

Prager EM, Bergstrom HC, Wynn GH, Braga MF (2016) The basolateral amygdala gamma-aminobutyric acidergic system in health and disease. J Neurosci Res 94(6):548–567. https://doi.org/10.1002/jnr.23690

Price JL, Russchen FT, Amaral DG (1987) The Limbic region. II: the amygdaloid complex. In: Björklund A, Hökfelt T, Swanson LW (eds) Handbook of chemical neuroanatomy, vol 5. Integrated systems of the CNS, Part I. Elsevier, Oxford, pp 279–388

Ramboz S, Oosting R, Amara DA, Kung HF, Blier P, Mendelsohn M, Mann JJ, Brunner D, Hen R (1998) Serotonin receptor 1A knockout: an animal model of anxiety-related disorder. Proc Natl Acad Sci USA 95:14476–14481

Rezayof A, Habibi P, Zarrindast MR (2011) Involvement of dopaminergic and glutamatergic systems of the basolateral amygdala in amnesia induced by the stimulation of dorsal hippocampal cannabinoid receptors. Neuroscience 175:118–126. https://doi.org/10.1016/j.neuroscience.2010.12.006

Rosene DL, Van Hoesen GW (1987) The hippocampal formation of the primate brain: a review of some comparative aspects of cytoarchitecture and connections. In: Jones EG, Peters A (eds) Cerebral cortex. Further aspects of cortical function, including hippocampus. Plenum Press, New York, pp 345–450

Rousseeuw PJ (1987) Silhouettes: a graphical aid to the interpretation and validation of cluster analysis. J Comput Appl Math 20:53–65

Simons LE, Moulton EA, Linnman C, Carpino E, Becerra L, Borsook D (2014) The human amygdala and pain: evidence from neuroimaging. Hum Brain Mapp 35(2):527–538. https://doi.org/10.1002/hbm.22199

Sims KS, Williams RS (1990) The human amygdaloid complex: a cytologic and histochemical atlas using Nissl, myelin, acetylcholinesterase and nicotinamide adenine dinucleotide phosphate diaphorase staining. Neuroscience 36:449–472

Sorvari H, Soininen H, Paljarvi L, Karkola K, Pitkanen A (1995) Distribution of parvalbumin-immunoreactive cells and fibers in the human amygdaloid complex. J Comp Neurol 360:185–212. https://doi.org/10.1002/cne.903600202

Sorvari H, Soininen H, Pitkanen A (1996a) Calbindin-D28K-immunoreactive cells and fibres in the human amygdaloid complex. Neuroscience 75:421–443

Sorvari H, Soininen H, Pitkanen (1996b) Calretinin-immunoreactive cells and fibers in the human amygdaloid complex. J Comp Neurol 369:188–208

Soudry Y, Lemogne C, Malinvaud D, Consoli SM, Bonfils P (2011) Olfactory system and emotion: common substrates. Eur Ann

Otorhinolaryngol Head Neck Dis 128:18–23. https://doi.org/10.1016/j.anorl.2010.09.007

Stefanacci L, Amaral DG (2002) Some observations on cortical inputs to the macaque monkey amygdala: an anterograde tracing study. J Comp Neurol 451:301–323. https://doi.org/10.1002/cne.10339

Stephan H (1975) Allocortex. Handbuch der mikroskopischen Anatomie des Menschen. Springer, Berlin

Svendsen CN, Bird ED (1985) Acetylcholinesterase staining of the human amygdala. Neurosci Lett 54:313–318

Takahashi H, Yamada M, Suhara T (2012) Functional significance of central D1 receptors in cognition: beyond working memory. J Cereb Blood Flow Metab 32:1248–1258. https://doi.org/10.1038/jcbfm.2011.194

Talarovicova A, Krskova L, Kiss A (2007) Some assessments of the amygdala role in suprahypothalamic neuroendocrine regulation: a minireview. Endocr Regul 41:155–162

Tanaka M, Yoshida M, Emoto H, Ishii H (2000) Noradrenaline systems in the hypothalamus, amygdala and locus coeruleus are involved in the provocation of anxiety: basic studies. Eur J Pharmacol 405:397–406

Walker DL, Davis M (2002) The role of amygdala glutamate receptors in fear learning, fear-potentiated startle, and extinction. Pharmacol Biochem Behav 71:379–392

Yilmazer-Hanke DM (2012) Amygdala. In: Mai JK, Paxinos G (eds) The human nervous system, 3rd edn. Elsevier, Amsterdam, pp 759–834

Zaborszky L, Hoemke L, Mohlberg H, Schleicher A, Amunts K, Zilles K (2008) Stereotaxic probabilistic maps of the magnocellular cell groups in human basal forebrain. Neuroimage 42:1127–1141. https://doi.org/10.1016/j.neuroimage.2008.05.055

Zilles K, Amunts K (2009) Receptor mapping: architecture of the human cerebral cortex. Curr Opin Neurol 22:331–339

Zilles K, Amunts K (2010) Centenary of Brodmann's map-conception and fate. Nat Rev Neurosci 11:139–145. https://doi.org/10.1038/nrn2776

Zilles K, Palomero-Gallagher N, Grefkes C, Scheperjans F, Boy C, Amunts K, Schleicher A (2002a) Architectonics of the human cerebral cortex and transmitter receptor fingerprints: reconciling functional neuroanatomy and neurochemistry. Eur Neuropsychopharmacol 12:587–599

Zilles K, Schleicher A, Palomero-Gallagher N, Amunts K (2002b) Quantitative analysis of cyto- and receptor architecture of the human brain. In: Mazziotta JC, Toga AW (eds) Brain mapping: the methods, 2nd edn. Elsevier, Amsterdam, pp 573–602

Zilles K, Bacha-Trams M, Palomero-Gallagher N, Amunts K, Friederici AD (2015) Common molecular basis of the sentence comprehension network revealed by neurotransmitter receptor fingerprints. Cortex 63:79–89. https://doi.org/10.1016/j.cortex.2014.07.007